

Data-Driven Mathematical Modeling Approaches for COVID-19: a survey

Jacques Demongeot¹, and Pierre Magal^{2,3,4,*}

- ¹ Université Grenoble Alpes, AGEIS EA7407, F-38700 La Tronche, France
- ² Department of Mathematics, Faculty of Arts and Sciences, Beijing Normal University, Zhuhai 519087, China
- ³ Univ. Bordeaux, IMB, UMR 5251, F-33400 Talence, France.
- ⁴ CNRS, IMB, UMR 5251, F-33400 Talence, France.
- * Correspondence: pierre.magal@u-bordeaux.fr

Abstract: In this review, we successively present the methods for phenomenological modeling of the evolution of reported and unreported cases of COVID-19, both in the exponential phase of growth and then in a complete epidemic wave. After the case of an isolated wave, we present the modeling of several successive waves separated by endemic stationary periods. Then, we treat the case of multi-compartmental models without or with age structure. Eventually, we review the literature, based on 230 articles selected in 11 sections, ranging from the medical survey of hospital cases to forecasting the dynamics of new cases in the general population.

Keywords: COVID-19 epidemic wave prediction; Epidemic models; Time series; Phenomenological models; Social changes; Time dependent models; Contagious disease; Endemic phase; Epidemic wave; Endemic/epidemic; Reported and unreported cases; Parameters identification;

I simply wish that, in a matter which so closely concerns the well-being of mankind, no decision shall be made without all the knowledge which a little analysis and calculation can provide, Daniel Bernoulli 1765.

Contents

1. Introduction	3	15
2. Reported and unreported data	3	16
2.1. What are the unreported cases?	3	17
2.2. Example of unreported cases	4	18
2.3. Testing data for New York state	4	19
3. Phenomenological models	6	20
4. Epidemic model with reported and unreported individuals	7	21
4.1. Mathematical model	7	22
4.2. Given Parameters	8	23
4.3. Computed parameters	8	24
5. Modeling the exponential phase	9	25
5.1. Initial number of infected and transmission rate	9	26
5.2. Application to COVID-19 in mainland China	9	27
5.3. Spectral method in epidemic time series	11	28
5.4. Monotone property of the cumulative distribution	12	29

Citation: Demongeot, J.; Magal, P. Data-Driven Mathematical Modeling Approaches for COVID-19: a survey. *Appl. Sci.* **2023**, *1*, 0. <https://doi.org/>

Received: September 2023

Revised:

Accepted:

Published:

Copyright: ©2023 by the authors. Submitted to *Appl. Sci.* for possible open access publication under the terms and conditions of the Creative Commons Attribution (CC BY) license (<https://creativecommons.org/licenses/by/4.0/>).

6. Modeling a single epidemic wave	14	30
6.1. What factors govern the transmission of pathogens	14	31
6.2. More results and references about the time dependent transmission rate modeling	15	33
6.3. Why do we need a time-dependent transmission rate?	16	34
6.4. Theoretical formula for $\tau(t)$	16	35
6.5. Explicit formula for $\tau(t)$ and I_0	18	36
6.6. Results	21	37
7. Modeling multiple epidemic waves	23	38
7.1. Phenomenological model used for multiple epidemic waves	23	39
7.2. Phenomenological Model apply to France	24	40
7.3. Phenomenological Model apply to several countries	25	41
7.4. Earlier results about transmission rate reconstructed from the data	26	42
7.5. Instantaneous reproduction number	26	43
7.6. Results	26	44
7.7. Consequences of the results	28	45
8. Exponential phase with more compartments	29	46
8.1. A model with transmission from the unreported infectious	29	47
8.2. The exponential phase approximation	29	48
8.3. Uncertainty due to the period chosen to fit the data	31	49
9. Modeling COVID-19 epidemic with age groups	32	50
9.1. Epidemic model with age groups	32	51
9.2. Cumulative reported cases with age structure in Japan	33	52
9.3. Method to Fit of the Age Structured Model to the Data	34	53
9.4. Rate of contact	34	54
10. A survey for COVID-19 mathematical modeling	37	55
10.1. Medical survey	37	56
10.2. Incubation, Infectiousness, and Recovery Period	38	57
10.3. Data	38	58
10.3.1. Contact tracing	38	59
10.3.2. Testing data	38	60
10.3.3. Unreported and uncertainty in the number of reported case data	38	61
10.3.4. Clusters	39	62
10.3.5. More phenomenological model to fit the data	39	63
10.3.6. Wasted water data	39	64
10.3.7. Discrete and random modeling	39	65
10.3.8. Time series and wavelet approaches	39	66
10.3.9. Transmission estimation and spatial modeling	39	67
10.3.10. Forecasting methods	40	68
10.4. SIR like models	40	69
10.4.1. Multigroups or multiscale models	40	70
10.4.2. Model with unreported or asymptomatic compartment	40	71
10.5. Connecting reported case data with SIR like model	40	72
10.6. Re-infections, natural and hybrid immunity	41	73
10.7. Mortality	41	74
10.8. Vaccination and mitigation measures	41	75
10.9. Chronological age	41	76
10.10. Basic reproduction number	42	77
10.11. Prediction of COVID-19 evolution	42	78
A. When the output is a single exponential function	43	79

B. References 44 80

1. Introduction 81

The COVID-19 outbreak has been the catalyst for increased scientific activity, particularly in data collection and modeling the dynamics of new cases and deaths due to the outbreak. 82
83
84

Such scientific excitement contemporary with a pandemic is not new. Several historical epidemic episodes have led to significant advances in public health, biostatistics, databases, and discrete or continuous mathematical modeling of disease evolution, considering the mechanisms of contagion, host resistance, and mutation of the infectious agent. Historically, we can thus distinguish several epidemic outbreaks followed by important scientific breakdowns: 85
86
87
88
89
90

A) The plague epidemic of 1348 saw the development of the beginnings of epidemiology with the recording of cases at the abbey of St Antoine (Isère in France) and in the network of hospitals managed by the Antonin monks; 91
92
93

B) During the London cholera epidemic of 1654, John Snow discovered the waterborne transmission of cholera, which led to significant changes to improve public health, notably by constructing improved sanitation facilities. This epidemic and its resolution by Snow even before the discovery of the responsible germ was a founding event in intervention epidemiology, with the validation of methods that can be applied to all diseases, not just contagious (infectious or social), in particular the principle of coupling the mapping of patients with that of sources of water for domestic consumption, which would later lead to the development of Geographic Information Systems (GIS) in epidemiology and to work such as the collection of water used as a COVID-19 tracer in the French Obépine project (<https://www.reseau-obepine.fr/>); 94
95
96
97
98
99
100
101
102
103

C) The smallpox epidemic of 1760 led to the importation into Europe of the inoculation practiced in Turkey (subsequently leading to vaccination by inert vaccine by Jenner) and to the creation of the first models for predicting epidemic waves by Bernoulli and d'Alembert. 104
105
106
107

In the tradition of these past discoveries, we will therefore present some recent progress in modeling the dynamics of infectious diseases and their transmission mechanisms in this article. 108
109
110

The plan of the paper is the following. Section 2 presents some background about the reported data. We explain some phenomena related to data collection, such as contact tracing, daily numbers of tests, and more. In section 3, we explain the main idea behind the notion of a phenomenological model. In section 4, we introduce an epidemic model with unreported cases and explain how to compare such a model with the data. In section 5, we consider the exponential phase of an epidemic, where the phenomenological model will be an exponential function. In section 6, we consider a single epidemic wave, where the phenomenological model will be the Boulli-Verhulst model. We consider several successive epidemic waves in section 7. In section 8, we present some new results to understand how to compare the data and the epidemic models with several compartments during the exponential phase. In section 9, we consider a model with age groups and explain how to deal with data in large systems. Section 10 is a survey section where we try to give some references for a selected number of important topics to model epidemic outbreaks. 111
112
113
114
115
116
117
118
119
120
121
122
123

2. Reported and unreported data 124

2.1. What are the unreported cases? 125

The unreported cases correspond to mild symptoms because people will only get tested in case of severe symptoms. Unreported cases can result from a lack of tests or asymptomatic patients [1]. That is infected patients that do not show symptoms. Unreported cases are partly due to a low daily number of tests. 126
127
128
129

2.2. Example of unreported cases

A published study traced COVID-19 infections resulting from a business meeting in Germany attended by a person who was infected but had no symptoms at the time [2]. Four people were eventually infected from this single contact.

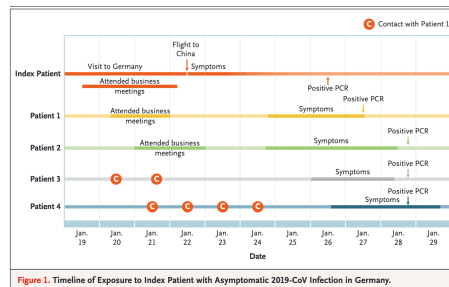


Figure 1. *Timeline of Exposure to Index Patient with Asymptomatic 2019-CoV Infection in Germany.*

A team in Japan [3] reports that 13 people evacuated from *Diamond Princess* were infected, 4 of whom, or 31 %, never developed symptoms.

On the French *aircraft carrier Charles de Gaulle*, clinical and biological data for all 1739 crew members were collected on arrival at the Toulon harbor and during quarantine: 1121 crew members (64%) were tested positive for COVID-19 using RT-PCR, and among these, 24% were asymptomatic [4].

2.3. Testing data for New York state

The goal of the figure below is to show that due to the changes in the method of detecting the cases, a jump occurred on February 12 in Wuhan in, China. The testing technology was not well developed at the early beginning of the epidemic, and such a problem also occurs in other countries.

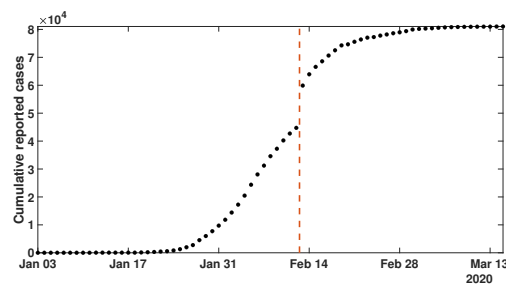


Figure 2. *Cumulative number of cases in Wuhan China.*

The dynamic of the daily number of tests is connected to the dynamic of the daily number of reported cases in a complex way [5].

The large peak in the number of tests at the end of April 2020, shows that the number of cases was strongly underestimated during the period. Because increasing the number of tests increases the number of positive test. Later on, the epidemic wave passed and the changes in the number of test had almost no influence on the number of positive test.

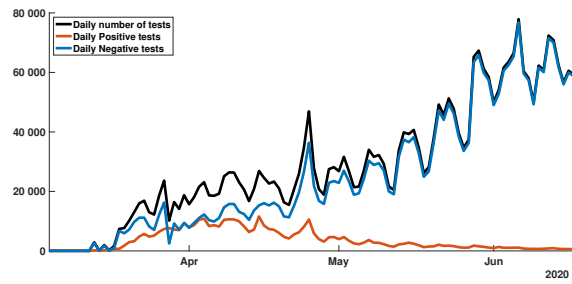


Figure 3. In this figure, we plot the daily number of tests for the New York State. The black curve, orange curve, and blue curve correspond respectively to the number of tests, the number of positive tests, and the number of negative tests.

The number of reported cases is the consequence of the combination of the dynamic of the number of tests (a complex dynamic which depends on human perceptions of the epidemic outbreak), and the dynamic of the epidemic outbreak (which is also very complex due the contact rate which depends on human perceptions) and the dynamic of transmission (which can also be complex due to the changes of susceptibility in the population).

Figure 4 presents the flowchart of the model used in [5]. In Figure 5 (which was obtained in [5]), we use the daily number of tests as an input of the model, and we fit the output of the model to the cumulative number of cases.

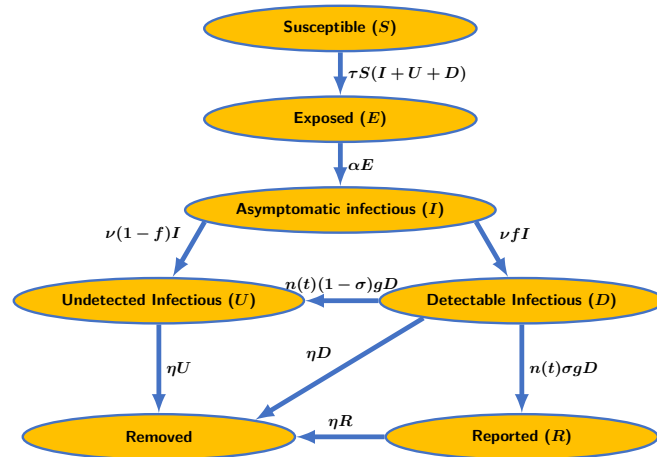


Figure 4. Flow chart of the epidemic model. In this diagram $n(t)$ is the daily number of tests at time t is an input of the model. We consider a fraction $(1 - \sigma)$ of false negative tests and a fraction σ of true positive tests. The parameter g reflects the fact that the tests are devoted not only to the symptomatic patients but also to a large fraction of the population of New York state.

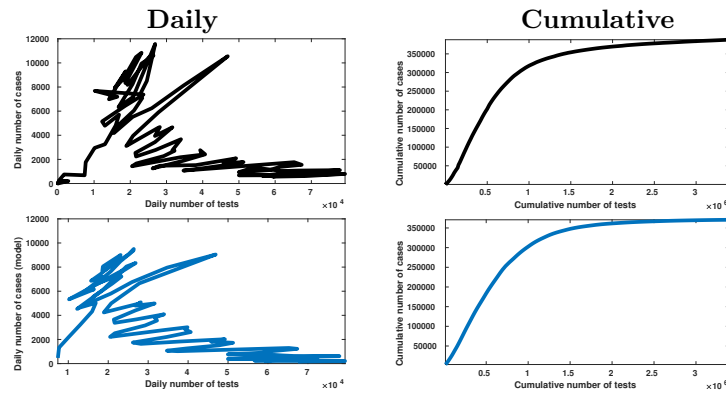


Figure 5. *The black curves are produced by using the New York state data only. The blue curves are constructed by using the model with the testing data as input of the model.*

In Figure 5, on the left-hand side, we consider the daily fluctuations of the number of reported cases (epidemic dynamic) and the daily number of tests (testing dynamics). Combining test dynamics and infection dynamics results in a complex time-parameterized curve. Nevertheless, we obtain a good correspondence between the top and the bottom left figures. The correspondence becomes excellent on the figures on the right, where we consider the cumulative number of declared cases and the cumulative number of tests.

3. Phenomenological models

Along this note, we use phenomenological models to fit the data.

Definition 1. *A phenomenological model is a mathematical model used to describe the data without mechanistic description of the processes involved in the phenomenon.*

In the next section, we will use exponential functions to get a continuous time representation of the data. This will be our first example of a phenomenological model. Our goal here is to replace the data by a function that captures the robust tendency of the phenomenon. In some sense, we are trying to get rid of the noise around the tendency.

By using, for example, spline functions, we can always fit the data perfectly. Then the fit is too precise to capture the significant information, and if we compute the derivatives of such a perfect fit, we will obtain a very noisy signal that is not meaningful.

Therefore the underlying idea of the phenomenological model is to derive a robust tendency with a limited number of parameters that will represent the data. Such a model is supposed to reduce the signal's noisy part and capture the robust part of the signal.

The phenomenological model can then replace the data, permitting analysis of some consequences when injected into the models. For example, we will obtain a meaningful range of parameters.

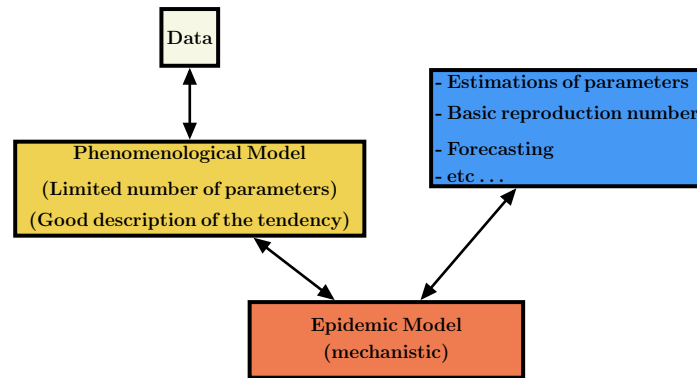


Figure 6. We can apply statistical methods to estimate the parameters of the proposed phenomenological model and derive their average values with some confidence intervals. The phenomenological model is used at the first step of the modelling process, providing regularized data to the epidemic model and allowing the identification of its parameters.

4. Epidemic model with reported and unreported individuals

4.1. Mathematical model

Transmissions between infectious and susceptible individuals are described by

$$\begin{cases} S'(t) = -\tau(t) S(t) I(t), \\ I'(t) = \tau(t) S(t) I(t) - \nu I(t), \end{cases} \quad (1)$$

where $S(t)$ is the number of susceptible and $I(t)$ the number of infectious at time t .

The system (1) is complemented with the initial data

$$S(t_0) = S_0 \geq 0, \text{ and } I(t_0) = I_0 \geq 0, \quad (2)$$

where t_0 is a time from which the epidemic model (1) becomes applicable.

In this model, the rate of transmission $\tau(t)$ combines the number of contacts per unit of time and the probability of transmission (see Section 6.1 for more information).

The number $1/\nu$ is the average duration of the asymptomatic infectious period, $\tau(t) S(t) I(t)$ is the flow of S -individuals becoming I -infected at time t . That is,

$$\int_{t_1}^{t_2} \tau(\sigma) S(\sigma) I(\sigma) d\sigma$$

is the number of individual that became I during the time interval $[t_1, t_2]$.

Similarly, $\nu I(t)$ is the flow of I -individuals leaving the I -compartment. That is

$$\int_{t_1}^{t_2} \nu I(\sigma) d\sigma$$

is the number of individual that became I during the time interval $[t_1, t_2]$.

The epidemic model associated with the flowchart in Figure 7 applies to the Hong Kong flu outbreak in New York City [6,7].

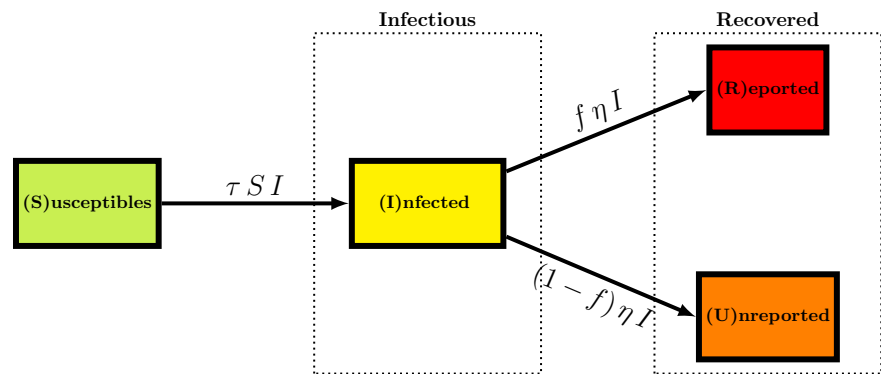


Figure 7. Flowchart.

We assume that the flow of reported individuals is a fraction $0 \leq f \leq 1$ of the flow of recovered individuals νI . That is,

$$\text{CR}'(t) = f \nu I(t), \text{ for } t \geq t_0, \quad (3)$$

where $\text{CR}(t)$ is the cumulative number of reported individuals, and f is the fraction of reported individuals. The fraction f is the fraction of patients with severe symptoms, and $1 - f$ the fraction of patients with mild symptoms.

4.2. Given Parameters

In this study, the following parameters will be given:

- Number of susceptible individuals when the epidemic starts

$$S_0 = 67 \text{ millions for France.}$$

- Time from which the epidemic model starts to be valid, also called initial time of the model t_0 .

Remark 2. The time t_0 is a time where the epidemic phase started already.

- The average duration of the infectiousness $\frac{4.1}{\nu} = 3 \text{ days.}$
- The fraction of reported individuals $f = 0.9.$

4.3. Computed parameters

The following parameters will be obtained by comparing the output of the model and the data:

- I_0 the number of asymptomatic infectious patients at the start of the epidemic.
- $\tau(t)$ the rate of transmission.

5. Modeling the exponential phase

At the early stage of the epidemic, we can assume that $S(t)$ is constant, and equal to S_0 . We can also assume that $\tau(t)$ remains constant equal to $\tau_0 = \tau(t_0)$. Therefore, by replacing these parameters into the I-equation of system (1) we obtain

$$I'(t) = (\tau_0 S_0 - \nu)I(t).$$

Therefore

$$I(t) = I_0 e^{\chi_2(t-t_0)}, \quad (4)$$

where

$$\chi_2 = \tau_0 S_0 - \nu. \quad (5)$$

5.1. Initial number of infected and transmission rate

By using (3) and (4), we obtain

$$\text{CR}(t) = \chi_1 \left(e^{\chi_2(t-t_0)} - 1 \right) + \chi_3. \quad (6)$$

We observe that

$$\text{CR}(t_0) = \chi_3,$$

then χ_3 is a parameter which must be estimated from the data.

By using (3) at t_0 , we obtain

$$I_0 = \frac{\text{CR}'(t_0)}{\nu f} = \frac{\chi_1 \chi_2}{\nu f}, \quad (7)$$

and by using (5)

$$\tau_0 = \frac{\chi_2 + \nu}{S_0}.$$

Note that the above estimations of I_0 and τ_0 are robust since we used the data over a period (i.e., not only at t_0) to evaluate χ_1, χ_2 .

5.2. Application to COVID-19 in mainland China

The figures below are taken from [8] (see [9] for similar results).

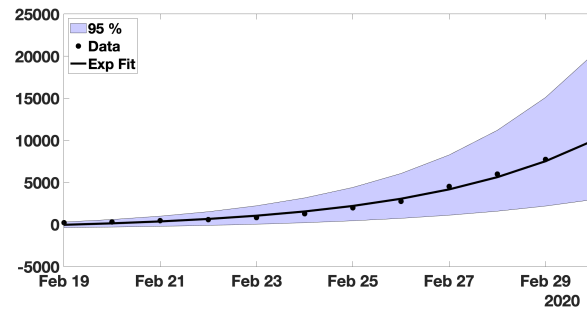


Figure 8. In this figure, we plot the best fit of the exponential model to the cumulative number of reported cases of COVID-19 in mainland China between February 19 and March 1. We obtain $\chi_1 = 3.7366$, $\chi_2 = 0.2650$ and $\chi_3 = 615.41$ with $t_0 = 19$ Feb. The parameter χ_3 is obtained by minimizing the error between the best exponential fit and the data.

Remark 3. Fixing $f = 0.5$ and $\nu = 0.2$, we obtain

$$I_0 = 3.7366 \times 0.2650 \times \exp(0.2650 \times 19) / (0.2 \times 0.5) = 1521,$$

and

$$\tau_0 = \frac{0.2650 + 0.2}{1.4 \times 10^9} = 3.3214 \times 10^{-10}.$$

One may compare Figure 2 with Figure 9 and realize that there is no more jump in Figure 9. Here, we canceled out the jump in Figure 2 due to a change of method in counting the number of cases. More precisely, on February 16, 2020, the cumulative data in Figure 2 jumps by 17409 cases (the original data are available in [10, Table 2]). From that day, public health authorities in China decided to include the patients showing symptoms.

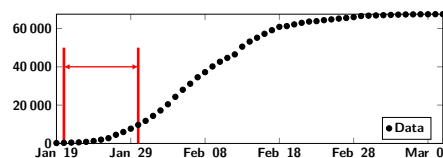


Figure 9. In this figure, the black dots represent the cumulative number of cases for China (with correction for the jump presented in Figure 2). The period marked in red corresponds to the period considered in Figure 8.

Remark 4. It is important to understand that, throughout this article, we fit the cumulative reported data by using a phenomenological. The reason is simple: the cumulative data are much smoother, while the daily number of reported cases are much more fluctuating. Therefore, it is "in theory" much easier to fit the cumulative data with a phenomenological model. Unfortunately, the problem is not that simple. So for example, in the exponential phase, we obtain the parameters

$$CR(t) = \chi_1 \left(e^{\chi_2(t-t_0)} - 1 \right) + \chi_3$$

by using a best fit to the cumulative number of cases.

Next, when we compute the first derivative of the above model to the daily number of cases, this gives a pretty reasonable approximation of the daily number of reported cases.

Another way to avoid the first derivative $t \rightarrow CR(t)$, is to use the following model

$$D'(t) = f\nu I(t) - D(t).$$

In this model, we use the same input flow of infected as for the model used to compute the cumulative number of cases. But here, we assume that daily cases individuals only stay one day in the D compartment. This model is also equivalent to

$$D(t) = e^{-(t-t_0)} D_0 + \int_{t_0}^t e^{-(t-\sigma)} f\nu I(\sigma) d\sigma,$$

and by replacing $f\nu I(\sigma)$ by the cumulative data $CR(\sigma)$, we obtain a formula for the daily number of cases. 230
231

So, during the exponential phase, once we obtain the best fit of the model to the cumulative data, the daily number of cases is given by

$$D(t) = e^{-(t-t_0)} D_0 + \int_{t_0}^t e^{-(t-\sigma)} \chi_1 \left(e^{\chi_2(\sigma-t_0)} - 1 \right) + \chi_3 d\sigma.$$

The model's advantage is that it avoids computing a derive of the cumulative number of cases, which can be an issue. 232
233

5.3. Spectral method in epidemic time series 234

During the COVID-19 pandemic, most people viewed the oscillations around the exponential growth at the beginning of an epidemic wave as the default in reporting the data. The residual is probably partly due to the reporting data process (random noise). Nevertheless, a significant remaining part of such oscillations could be connected to the infection dynamic at the level of a single average patient. Eventually, the central question we try to address here is: Is there some hidden information in the signal around the exponential tendency for COVID-19 data? So we consider the early stage of an epidemic phase, and we try to exploit the oscillations around the tendency in order to reconstruct the infection dynamic at the level of a single average patient. We investigate this question in [11]. 235
236
237
238
239
240
241
242
243

The figures below are taken from [11, see Figures 13 and 14]. 244

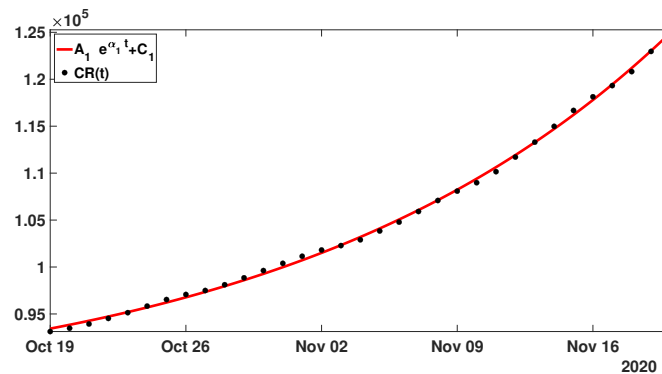


Figure 10. In this figure, we plot the cumulative number of reported cases data for Japan between 19 October and 19 November 2020 (black dots). We plot the best fit of the model (29) to the cumulative data (red curve).

Then in the figure below we plot the first residual. That is,

$$\text{Residual}_1(t) = CR(t) - [A_1 e^{\alpha_1 t} + C_1].$$

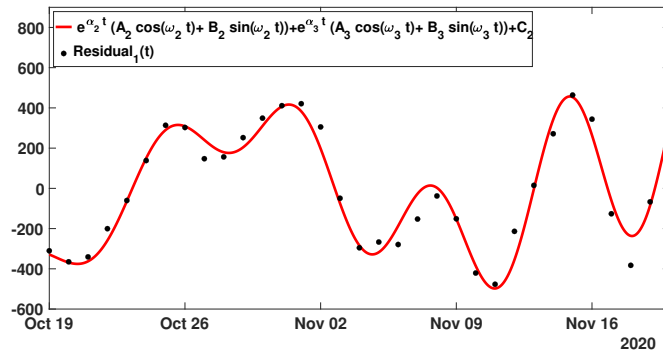


Figure 11. In this figure, we plot the first residual when subtracting the exponential tendency obtained in Figure 9 to the cumulative reported cases data between 19 October and 19 November 2020 (black dots). We plot the best fit of the model to the first residual (red curve).

5.4. Monotone property of the cumulative distribution

The influence of the errors made in the estimations (at the early stage of the epidemic) has been considered in the recent article [12]. To understand this problem, let us first consider the case of the rate of transmission $\tau(t) = \tau_0$ in the model (1).

From the epidemic model to the data Assume that the transmission rate $\tau(t)$ is constant equal to $\tau > 0$ in the model (1). Then by integrating the S -equation in model (1) between t_0 and t , we obtain

$$S(t) = S_0 e^{\tau CI(t)} \tag{8}$$

where

$$CI(t) = \int_{t_0}^t I(\sigma) d\sigma.$$

Moreover

$$I'(t) = \tau S(t)I(t) - \nu I(t).$$

replacing $S(t)$ by 8, and by integrating between t_0 and t we obtain

$$I(t) = I_0 + S_0 \left(1 - e^{-\tau CI(t)} \right) - \nu CI(t).$$

Remembering that $CI(t)' = I(t)$, we conclude that the cumulative number of cases should follow a single ordinary differential equation

$$CI(t)' = I_0 + S_0 \left(1 - e^{-\tau CI(t)} \right) - \nu CI(t). \tag{9}$$

The system (9) is complemented with the initial distribution of the model

$$CI(t_0) = CI_0 \geq 0.$$

This equation should be a good phenomenological model whenever $t \mapsto \tau(t)$ is a constant function. We refer to [13], and [14, Chapter 8] for a comprehensive presentation on the monotone ordinary differential equations.

Theorem 5. Let $t > t_0$ be fixed. The cumulative number of infectious $CI(t)$ is strictly increasing with respect to the following quantities

- (i) $I_0 > 0$ the initial number of infectious individuals;
- (ii) $S_0 > 0$ the initial number of susceptible individuals;
- (iii) $\tau > 0$ the transmission rate;

(iv) $1/\nu > 0$ the average duration of the infectiousness period.

262

Error in the estimated initial number of infected and transmission rate

Assume that the parameters χ_1 and χ_2 are estimated with a 95% confidence interval

$$\chi_{1,95\%}^- \leq \chi_1 \leq \chi_{1,95\%}^+,$$

and

$$\chi_{2,95\%}^- \leq \chi_2 \leq \chi_{2,95\%}^+.$$

We obtain

$$I_{0,95\%}^- := \frac{\chi_{1,95\%}^- \chi_{2,95\%}^- e^{\chi_{2,95\%}^- t_0}}{\nu f} \leq I_0 \leq I_{0,95\%}^+ := \frac{\chi_{1,95\%}^+ \chi_{2,95\%}^+ e^{\chi_{2,95\%}^+ t_0}}{\nu f},$$

and

$$\tau_{0,95\%}^- := \frac{\chi_{2,95\%}^- + \nu}{S_0} \leq \tau_0 \leq \tau_{0,95\%}^+ := \frac{\chi_{2,95\%}^+ + \nu}{S_0}.$$

263

Remark 6. By using the data for mainland China we obtain

$$\chi_{1,95\%}^- = 1.57, \chi_{1,95\%}^+ = 5.89, \chi_{2,95\%}^- = 0.24, \chi_{2,95\%}^+ = 0.28.$$

In Figure 12, we plot the upper and lower solutions $CR^+(t)$ (obtained by using $I_0 = I_{0,95\%}^+$ and $\tau_0 = \tau_{0,95\%}^+$) and $CR^-(t)$ (obtained by using $I_0 = I_{0,95\%}^-$ and $\tau_0 = \tau_{0,95\%}^-$) corresponding to the blue region and the black curve corresponds to the best estimated values $I_0 = 1521$ and $\tau_0 = 3.3214 \times 10^{-10}$.

264

265

266

267

Recall that the final size of the epidemic corresponds to the positive equilibrium of (9)

$$0 = I_0 + S_0[1 - \exp(-\tau_0 CI_\infty)] - \nu CI_\infty.$$

In Figure 12 the changes in the parameters I_0 and τ_0 (in (5.4)-(5.4)) do not affect significantly the final size.

268

269

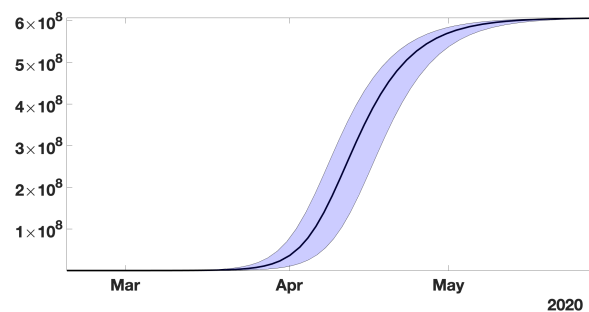


Figure 12. In this figure, the black curve corresponds to the cumulative number of reported cases $CR(t)$ obtained from the model (7) with $CR'(t) = \nu f I(t)$ by using the values $I_0 = 1521$ and $\tau_0 = 3.32 \times 10^{-10}$ obtained from our method and the early data from February 19 to March 1. The blue region corresponds the 95% confidence interval when the rate of transmission $\tau(t)$ is constant and equal to the estimated value $\tau_0 = 3.32 \times 10^{-10}$.

Remark 7. Theorem 5 can be used day by day to fit the cumulative number of infected $CI(t)$. Indeed, if we assume that $\tau(t)$ is a day-by-day piece-wise constant, we can use the monotone properties to find a unique daily value for τ to fit the cumulative data to obtain a perfect match. Such an algorithm was developed in [8].

270

271

272

273

6. Modeling a single epidemic wave

6.1. What factors govern the transmission of pathogens

Estimating the average transmission rate is one of the most crucial challenges in the epidemiology of communicable diseases. This rate conditions the entry into the epidemic phase of the disease and its return to the extinction phase, if it has diminished sufficiently. It is the combination of three factors, one, the coefficient of virulence, linked to the infectious agent (in the case of infectious transmissible diseases), the other, the coefficient of susceptibility, linked to the host (all summarized into the probability of transmission), and also, the number of contact per unit of time between individuals (see [15]). The coefficient of virulence may change over time due to mutation over the course of the disease history. The second and third also, if mitigation measures have been taken. This was the case in China from the start of the pandemic (see [16]). Monitoring the decrease in the average transmission rate is an excellent way to monitor the effectiveness of these mitigation measures. Estimating the rate is therefore a central problem in the fight against epidemics.

The transmission rate may vary over time, and it may significantly impact epidemic outbreaks. As explained in [15], the transmission rate can be decomposed as follow

$$\tau(t) = \frac{\text{the probability of transmission}}{\text{the average duration of a contact}}.$$

In this formula, the transmission probability may depend on climatic changes (temperature, humidity, ultraviolet, and other external factors), and the average duration of contact depends on human social behavior. It can be noted that the transmission rate is proportional to the inverse of the average contact duration because the shorter the average contact duration, the greater the number of contacts per unit of time.

Remark 8. A model was proposed by [17] to describe the evolution of the transmission rate during a single epidemic wave. Namely, the model is the following

$$\tau(t) = \begin{cases} \tau_0, & \text{if } t_0 \leq t \leq N, \\ \tau_0 \left(p e^{-\mu(t-N)} + (1-p) \right), & \text{if } t \geq N, \end{cases}$$

where N corresponds to the day when the public measures take effect, and μ is the rate at which they take effect (this parameter describes the speed at which the public measures are taking place). The fraction $0 \leq p \leq 1$ is the fraction by which the transmission rate is reduced when applying public measures. We can rewrite this model shortly by using $t^+ = \max(t, 0)$, the positive part of t . That is,

$$\tau(t) = \tau_0 \left(p e^{-\mu(t-N)^+} + (1-p) \right),$$

Such a model was successfully used by [10,18–20] and others.

Nevertheless, the model for joining the end of an epidemic wave to the next epidemic wave is still unknown. A tentative model was proposed in [18].

Contact patterns are impacted by social distancing measures. The average number of contacts per unit of time depends on the density of population [21,22]. The probability of transmission depends of the virulence of the pathogen which can depend on the temperature, the humidity, and the Ultraviolet [23,24]. In COVID-19 the level of susceptibility may depend on blood group and genetic lineage. It is indeed suspected that the

- Blood group[25] : Blood group O is associated with a lower susceptibility to SARS-CoV2;

- Genetic lineage [26] A gene cluster inherited from Neanderthal has been identified as a risk factor for severe symptoms.

6.2. More results and references about the time dependent transmission rate modeling

Throughout this section, the parameter $S_0 = 1.4 \times 10^9$ will be the entire population of mainland China (since COVID-19 is a newly emerging disease). The actual number of susceptibles S_0 can be smaller since some individuals can be partially (or totally) immunized by previous infections or other factors. This is also true for Sars-CoV2, even if COVID-19 is a newly emerging disease.

At the early beginning of the epidemic, the average duration of the infectious period $1/\nu$ is unknown, since the virus has never been investigated in the past. Therefore, at the early beginning of the COVID-19 epidemic, medical doctors and public health scientists used previously estimated average duration of the infectious period to make some public health recommendations. Here we show that the average infectious period is impossible to estimate by using only the time series of reported cases, and must therefore be identified by other means. Actually, with the data of Sars-CoV2 in mainland China, we will fit the cumulative number of the reported case almost perfectly for any non-negative value $1/\nu < 3.3$ days. In the literature, several estimations were obtained: 11 days in [27], 9.5 days in [28], 8 days in [29], and 3.5 days in [30]. The recent survey by Byrne et al. [31] focuses on this subject.

Result

In Section 6.4, our analysis shows that

- It is hopeless to estimate the exact value of the duration of infectiousness by using SI models. Several values of the average duration of the infectious period give the exact same fit to the data.
- We can estimate an upper bound for the duration of infectiousness by using SI models. In the case of Sars-CoV2 in mainland China, this upper bound is 3.3 days.

In [2], it is reported that transmission of COVID-19 infection may occur from an infectious individual who is not yet symptomatic. In [32], it is reported that COVID-19 infected individuals generally develop symptoms, including mild respiratory symptoms and fever, on average 5 – 6 days after the infection date (with a confidence of 95%, range 1 – 14 days). In [33], it is reported that the median time prior to symptom onset is 3 days, the shortest 1 day, and the longest 24 days. It is evident that these time periods play an important role in understanding COVID-19 transmission dynamics. Here the fraction of reported individuals f is unknown as well.

Result

In Section 6.4, our analysis shows that:

- It is hopeless to estimate the fraction of reported by using the SI models. Several values for the fraction of reported give the exact same fit to the data.
- We can estimate a lower bound for the fraction of unreported. We obtain $3.83 \times 10^{-5} < f \leq 1$. This lower bound is not significant. Therefore we can say anything about the fraction of unreported from this class of models.

As a consequence, the parameters $1/\nu$ and f have to be estimated by another method, for instance by a direct survey methodology that should be employed on an appropriated sample in the population in order to evaluate the two parameters.

The goal of this section is to focus on the estimation of the two remaining parameters. Namely, knowing the above-mentioned parameters, we plan to identify

- I_0 the initial number of infectious at time t_0 ;

- $\tau(t)$ the rate of transmission at time t .

This problem has already been considered in several articles. In the early 70s, London and Yorke [34,35] already discussed the time dependent rate of transmission in the context of measles, chickenpox and mumps. More recently, [36] the question of reconstructing the rate of transmission was considered for the 2002-2004 SARS outbreak in China. In [17] a specific form was chosen for the rate of transmission and applied to the Ebola outbreak in Congo. Another approach was also proposed in [37].

6.3. Why do we need a time-dependent transmission rate?

In Figure 13, we observe that the SI model with a constant transmission rate initially fits the data well. With this choice of parameters, the SI model is also supposed with the exponential function. But the model and the exponential function diverge relatively rapidly from the data. It is easy to understand that once people were informed about the COVID-19 outbreak, they tried to protect themselves, and the number of contacts per unit of time then reduced gradually. That is, the transmission rate gradually decreased.

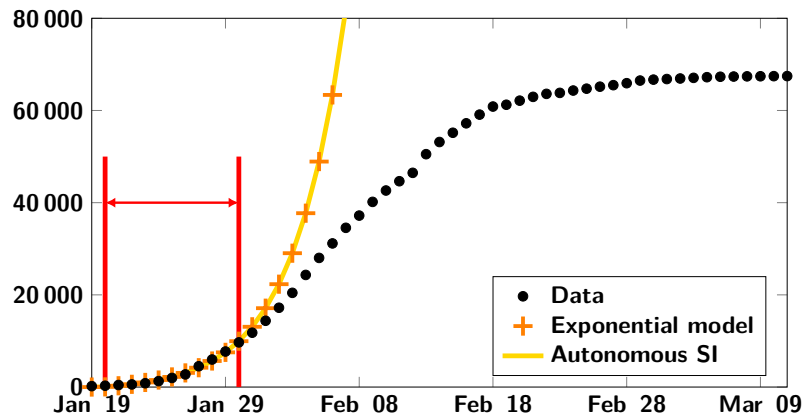


Figure 13. In this figure, the black dots represent the cumulative number of cases for China (we a correction for the jump presented in Figure 2). The period marked in red corresponds to the period considered in Figure 8. The yellow curve corresponds to the number of infected obtained using model (1) with a constant rate of transmission $\tau(t)$. We observe a rapid divergence between the epidemic model and the data whenever the transmission rate is constant with time.

6.4. Theoretical formula for $\tau(t)$

By using the S-equation of model (1) we obtain

$$S(t) = S_0 \exp\left(-\int_{t_0}^t \tau(\sigma) I(\sigma) d\sigma\right),$$

next by using the I-equation of model (1) we obtain

$$I'(t) = S_0 \exp\left(-\int_{t_0}^t \tau(\sigma) I(\sigma) d\sigma\right) \tau(t) I(t) - \nu I(t),$$

and by taking the integral between t and t_0 we obtain a Volterra integral equation for the cumulative number of infectious

$$CI'(t) = I_0 + S_0 \left[1 - \exp\left(-\int_{t_0}^t \tau(\sigma) I(\sigma) d\sigma\right)\right] - \nu CI(t), \quad (10)$$

which is equivalent to (by using (3))

$$\text{CR}'(t) = \nu f \left(I_0 + S_0 \left[1 - \exp \left(-\frac{1}{\nu f} \int_{t_0}^t \tau(\sigma) \text{CR}'(\sigma) d\sigma \right) \right] \right) + \nu \text{CR}_0 - \nu \text{CR}(t). \quad (11)$$

The following result permits to obtain a perfect match between the SI model and the time-dependent rate of transmission $\tau(t)$.

Theorem 9. *Let $S_0, \nu, f, I_0 > 0$ and $\text{CR}_0 \geq 0$ be given. Let $t \rightarrow I(t)$ be the second component of system (1). Let $\widehat{\text{CR}} : [t_0, \infty) \rightarrow \mathbb{R}$ be a two times continuously differentiable function satisfying*

$$\widehat{\text{CR}}(t_0) = \text{CR}_0, \quad (12)$$

$$\widehat{\text{CR}}'(t_0) = \nu f I_0, \quad (13)$$

$$\widehat{\text{CR}}'(t) > 0, \forall t \geq t_0, \quad (14)$$

and

$$\nu f (I_0 + S_0) - \widehat{\text{CR}}'(t) - \nu (\widehat{\text{CR}}(t) - \text{CR}_0) > 0, \forall t \geq t_0. \quad (15)$$

Then

$$\widehat{\text{CR}}(t) = \text{CR}_0 + \nu f \int_{t_0}^t I(s) ds, \forall t \geq t_0, \quad (16)$$

if and only if

$$\tau(t) = \frac{\nu f \left(\frac{\widehat{\text{CR}}''(t)}{\widehat{\text{CR}}'(t)} + \nu \right)}{\nu f (I_0 + S_0) - \widehat{\text{CR}}'(t) - \nu (\widehat{\text{CR}}(t) - \text{CR}_0)}. \quad (17)$$

Proof. Assume first (16) is satisfied. Then by using equation (10) we deduce that

$$S_0 \exp \left(- \int_{t_0}^t \tau(\sigma) I(\sigma) d\sigma \right) = I_0 + S_0 - I(t) - \nu \text{CI}(t).$$

Therefore

$$\int_{t_0}^t \tau(\sigma) I(\sigma) d\sigma = \ln \left[\frac{S_0}{I_0 + S_0 - I(t) - \nu \text{CI}(t)} \right] = \ln(S_0) - \ln[I_0 + S_0 - I(t) - \nu \text{CI}(t)]$$

therefore by taking the derivative on both side

$$\tau(t) I(t) = \frac{I'(t) + \nu I(t)}{I_0 + S_0 - I(t) - \nu \text{CI}(t)} \Leftrightarrow \tau(t) = \frac{\frac{I'(t)}{I(t)} + \nu}{I_0 + S_0 - I(t) - \nu \text{CI}(t)} \quad (18)$$

and by using the fact that $\text{CR}(t) - \text{CR}_0 = \nu f \text{CI}(t)$ we obtain (17).

Conversely, assume that $\tau(t)$ is given by (17). Then if we define $\tilde{I}(t) = \widehat{\text{CR}}'(t) / \nu f$ and $\tilde{\text{CI}}(t) = (\widehat{\text{CR}}(t) - \text{CR}_0) / \nu f$, by using (12) we deduce that

$$\tilde{\text{CI}}(t) = \int_{t_0}^t \tilde{I}(\sigma) d\sigma,$$

and by using (13)

$$\tilde{I}(t_0) = I_0. \quad (19)$$

Moreover from (17) we deduce that $\tilde{I}(t)$ satisfies (18). By using (19) we deduce that $t \rightarrow \tilde{CI}(t)$ is a solution of (10). By uniqueness of the solution of (10), we deduce that $\tilde{CI}(t) = CI(t), \forall t \geq t_0$ or equivalently $CR(t) = CR_0 + \nu f \int_{t_0}^t I(s) ds, \forall t \geq t_0$. The proof is completed. \square

The formula (17) was already obtained by Haderler [38, see Corollary 2].

6.5. Explicit formula for $\tau(t)$ and I_0

In 1766, Bernoulli [39] investigated an epidemic phase followed by an endemic phase. This appears clearly in Figures 9 and 10 in [40] who revisited the original article of Bernoulli. We also refer to [41] for another article revisiting the original work of Bernoulli. A similar article has been re-written in French as well by [42]. In 1838, Verhulst [43] introduced the same equation to describe population growth. Several works comparing cumulative reported cases data and the Bernoulli–Verhulst model appear in the literature (see [44–46]). The Bernoulli–Verhulst model is sometimes called Richard’s model, although Richard’s work came much later in 1959.

Many phenomenological models have been compared to the data during the first phase of the COVID-19 outbreak. We refer to the paper of [47] for a nice survey on the generalized logistic equations. Let us consider here for example, the Bernoulli-Verhulst equation

$$CR'(t) = \chi_2 CR(t) \left(1 - \left(\frac{CR(t)}{CR_\infty} \right)^\theta \right), \forall t \geq t_0, \quad (20)$$

supplemented with the initial data

$$CR(t_0) = CR_0 \geq 0.$$

Let us recall the explicit formula for the solution of (20)

$$CR(t) = \frac{e^{\chi_2(t-t_0)} CR_0}{\left[1 + \frac{\chi_2 \theta}{CR_\infty^\theta} \int_{t_0}^t (e^{\chi_2(\sigma-t_0)} CR_0)^\theta d\sigma \right]^{1/\theta}} = \frac{e^{\chi_2(t-t_0)} CR_0}{\left[1 + \frac{CR_0^\theta}{CR_\infty^\theta} (e^{\chi_2 \theta(t-t_0)} - 1) \right]^{1/\theta}}. \quad (21)$$

The model’s main advantage is that it is rich enough to fit the data, together with a limited number of parameters. To fit this model to the data, we only need to estimate four parameters χ_2, θ, CR_0 , and CR_∞ .

Remark 10. *Plenty of possibilities exist to fit the data, including split functions (irregular functions with many parameters) and others. In [48], they proposed several possible alternatives, including a generalized logistic equation of the form*

$$CR'(t) = \chi_2 CR(t)^\theta \left(1 - \left(\frac{CR(t)}{CR_\infty} \right) \right), \forall t \geq t_0.$$

The above equation has no explicit solution. Therefore it is more difficult to use it than the Bernoulli-Verhulst model. We also refer to [49,50] for more phenomenological model to fit an epidemic wave.

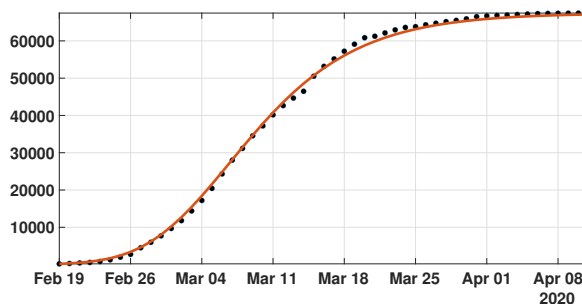


Figure 14. In this figure, we plot the best fit of the Bernoulli-Verhulst model to the cumulative number of reported cases of COVID-19 in China. We obtain $\chi_2 = 0.66$ and $\theta = 0.22$. The black dots correspond to data for the cumulative number of reported cases and the red curve corresponds to the model.

Estimated initial number of infected

By combining (10) and the Bernoulli-Verhulst equation (20) for $t \rightarrow CR(t)$, we deduce the initial number of infected

$$I_0 = \frac{CR'(t_0)}{\nu f} = \frac{\chi_2 CR_0 \left(1 - \left(\frac{CR_0}{CR_\infty}\right)^\theta\right)}{\nu f}. \tag{22}$$

392

Remark 11. We fix $f = 0.5$, from the COVID-19 data in mainland China and formula (22) (with $CR_0 = 198$), we obtain

$$I_0 = 1909 \text{ for } \nu = 0.1,$$

and

$$I_0 = 954 \text{ for } \nu = 0.2.$$

By using (20) we deduce that

$$\begin{aligned} CR''(t) &= \chi_2 CR'(t) \left(1 - \left(\frac{CR(t)}{CR_\infty}\right)^\theta\right) - \frac{\chi_2 \theta}{CR_\infty^\theta} CR(t) (CR(t))^{\theta-1} CR'(t) \\ &= \chi_2 CR'(t) \left(1 - \left(\frac{CR(t)}{CR_\infty}\right)^\theta\right) - \frac{\chi_2 \theta}{CR_\infty^\theta} (CR(t))^\theta CR'(t), \end{aligned}$$

therefore

$$CR''(t) = \chi_2 CR'(t) \left(1 - (1 + \theta) \left(\frac{CR(t)}{CR_\infty}\right)^\theta\right). \tag{23}$$

393

Estimated rate of transmission

By using the Bernoulli-Verhulst equation (20) and substituting (23) in (17), we obtain

$$\tau(t) = \frac{\nu f \left(\chi_2 \left(1 - (1 + \theta) \left(\frac{\text{CR}(t)}{\text{CR}_\infty} \right)^\theta \right) + \nu \right)}{\nu f(I_0 + S_0) + \nu \text{CR}_0 - \text{CR}(t) \left(\chi_2 \left(1 - \left(\frac{\text{CR}(t)}{\text{CR}_\infty} \right)^\theta \right) + \nu \right)}. \quad (24)$$

This formula (24) combined with (21) gives an explicit formula for the rate of transmission.

Since $\text{CR}(t) < \text{CR}_\infty$, by considering the sign of the numerator and the denominator of (24), we obtain the following proposition.

Proposition 12. *The rate of transmission $\tau(t)$ given by (24) is non negative for all $t \geq t_0$ if*

$$\nu \geq \chi_2 \theta, \quad (25)$$

and

$$f(I_0 + S_0) + \nu \text{CR}_0 > \text{CR}_\infty (\chi_2 + \nu). \quad (26)$$

Compatibility of the model SI with the COVID-19 data for mainland China

The model SI is compatible with the data only when $\tau(t)$ stays positive for all $t \geq t_0$. From our estimation of the Chinese's COVID-19 data we obtain $\chi_2 \theta = 0.14$. Therefore from (25) we deduce that model is compatible with the data only when

$$1/\nu \leq 1/0.14 = 3.3 \text{ days}. \quad (27)$$

This means that the average duration of infectious period $1/\nu$ must be shorter than 3.3 days.

Similarly the condition (26) implies

$$f \geq \frac{\text{CR}_\infty \chi_2 + (\text{CR}_\infty - \text{CR}_0) \nu}{S_0 + I_0} \geq \frac{\text{CR}_\infty \chi_2 + (\text{CR}_\infty - \text{CR}_0) \chi_2 \theta}{S_0 + I_0}$$

and since we have $\text{CR}_0 = 198$ and $\text{CR}_\infty = 67102$, we obtain

$$f \geq \frac{67102 \times 0.66 + (67102 - 198) \times 0.14}{1.4 \times 10^9} \geq 3.83 \times 10^{-5}. \quad (28)$$

So according to this estimation the fraction of unreported $0 < f \leq 1$ can be almost as small as we want.

Figure 15 illustrates the Proposition 12. We observe that the formula for the rate of transmission (24) becomes negative whenever $\nu < \chi_2 \theta$.

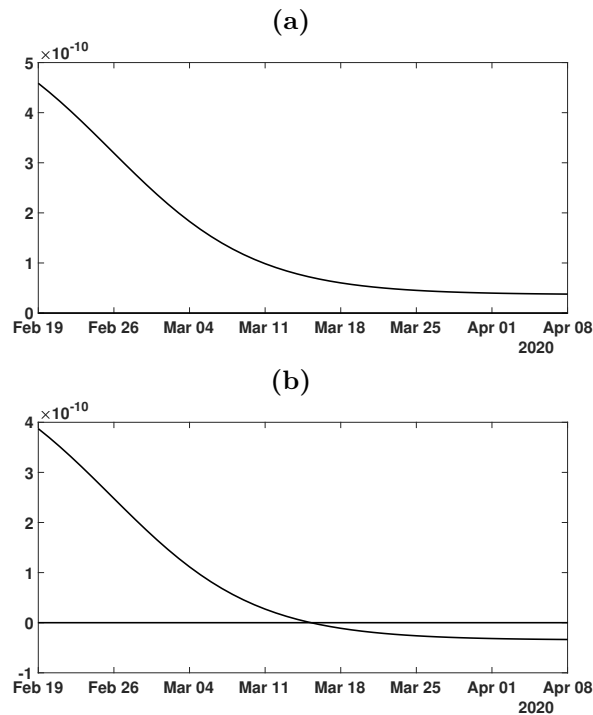


Figure 15. In this figure, we plot the rate of transmission obtained from formula (24) with $f = 0.5$, $\chi_2\theta = 0.14 < \nu = 0.2$ (in Figure (a)) and $\nu = 0.1 < \chi_2\theta = 0.14$ (in Figure (b)), $\chi_2 = 0.66$ and $\theta = 0.22$ and $CR_\infty = 67102$ which is the latest value obtained from the cumulative number of reported cases for China.

In Figure 16 we plot the numerical simulation obtained from (1)-(3) when $t \rightarrow \tau(t)$ is replaced by the explicit formula (24). It is surprising that we can reproduce perfectly the original Bernoulli-Verhulst even when $\tau(t)$ becomes negative. This was not guaranteed at first, since the I-class of individuals is losing some individuals which are recovering.

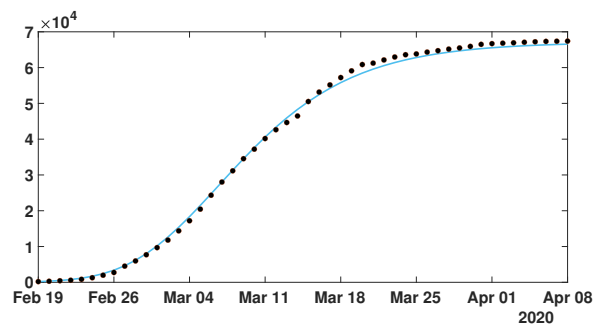


Figure 16. In this figure, we plot the number of reported cases by using model (1) and (10), and the rate of transmission is obtained in (24). The parameters values are $f = 0.5$, $\nu = 0.1$ or $\nu = 0.2$, $\chi_2 = 0.66$ and $\theta = 0.22$ and $CR_\infty = 67102$ is the latest value obtained from the cumulative number of reported cases for China. Furthermore, we use $S_0 = 1.4 \times 10^9$ for the total population of China and $I_0 = 954$ which is obtained from formula (22). The black dots correspond to data for the cumulative number of reported cases observed and the blue curve corresponds to the model.

6.6. Results

In [8], we designed an algorithm, based on the monotone property described in Theorem 5 to recover the transmission rate from the data. In this section, we reconsider the result presented in [8] where several method was used to regularized the data.

In Figure 17 we plot several types of regularized cumulative data in figure (a) and several types of regularized daily data in figure (b). Among the different regularization methods, an important one is the Bernoulli-Verhulst best fit approximation.

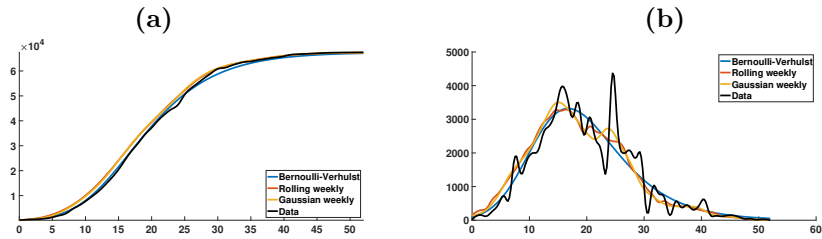


Figure 17. In this figure, we plot the cumulative number of reported cases (left) and the daily number of reported cases (right). The black curves are obtained by applying the cubic spline matlab function `"spline(Days,DATA)"` to the cumulative data. The left-hand side is obtained by using the cubic spline function and right-hand side is obtained by using the derivative of the cubic spline interpolation. The blue curves are obtained by using cubic spline function to the day by day values of cumulative number of cases obtained from the best fit of the Bernoulli-Verhulst model. The orange curves are obtained by computing the rolling weekly daily number of cases (we use the matlab function `"smoothdata(DAILY,'movmean',7)"`) and then by applying the cubic spline function the corresponding cumulative number of cases. The yellow curves are obtained by Gaussian the rolling weekly to the daily number of cases (we use the matlab function `"smoothdata(DAILY,'gaussian',7)"`) and then by applying the cubic spline function to the corresponding cumulative number of cases.

In Figure 18 we plot the rate of transmission $t \rightarrow \tau(t)$ obtained by using Algorithm 2. We can see that the original data gives a negative transmission rate while at the other extreme the Bernoulli-Verhulst seems to give the most regularized transmission rate. In Figure 18-(a) we observe that we now recover almost perfectly the theoretical transmission rate obtained in (24). In Figure 18-(b) the rolling weekly average regularization and in Figure 18-(c) the Gaussian weekly average regularization still vary a lot and in both cases the transmission rate becomes negative after some time. In Figure 18-(c) the original data gives a transmission rate that is negative from the beginning. We conclude that it is crucial to find a "good" regularization of the daily number of case. So far the best regularization method is obtained by using the best fit of the Bernoulli-Verhulst model.

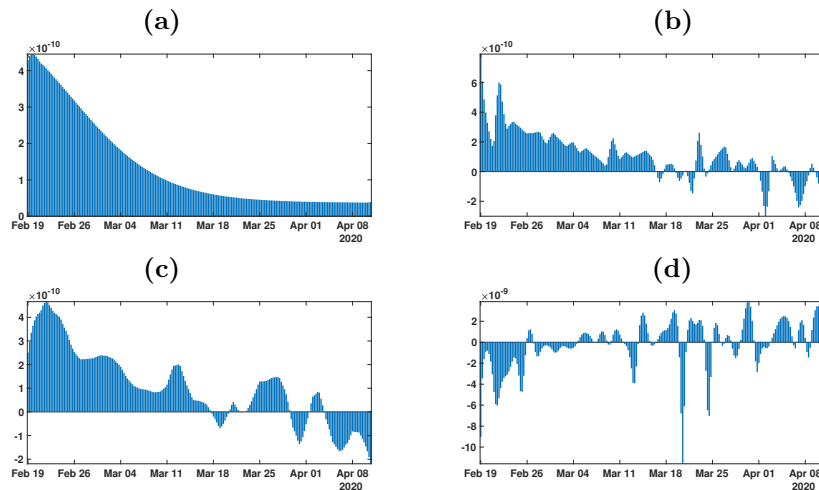


Figure 18. In this figure we plot the transmission rates $t \rightarrow \tau(t)$ obtained by using Algorithm 2 with the parameters $f = 0.5$ and $\nu = 0.2$. In figure (a) we use the cumulative data obtained by using the Bernoulli-Verhulst regularization. In figure (b) we use the cumulative data obtained by using the rolling weekly average regularization. In figure (c) we use the cumulative data obtained by using the Gaussian weekly average regularization. In figure (d) we use the original cumulative data.

7. Modeling multiple epidemic waves

7.1. Phenomenological model used for multiple epidemic waves

Endemic phase: During the endemic phase, the dynamics of new cases appears to fluctuate around an average value independently of the number of cases. Therefore the average cumulative number of cases is given by

$$\text{CR}(t) = N_0 + (t - t_0) \times a, \text{ for } t \in [t_0, t_1], \quad (29)$$

where t_0 denotes the beginning of the endemic phase, N_0 is the number of new cases at time t_0 , and a is the average value of the daily number of new cases.

Epidemic phase: In the epidemic phase, the new cases are contributing to produce secondary cases. Therefore the daily number of new cases is no longer constant, but varies with time as follows

$$\text{CR}(t) = N_{\text{base}} + \frac{e^{\chi(t-t_0)} N_0}{\left[1 + \frac{N_0^\theta}{N_\infty^\theta} (e^{\chi\theta(t-t_0)} - 1)\right]^{1/\theta}}, \text{ for } t \in [t_0, t_1]. \quad (30)$$

In other words, the daily number of new cases follows the Bernoulli-Verhulst equation. That is,

$$N(t) = \text{CR}(t) - N_{\text{base}}, \quad (31)$$

we obtain

$$N'(t) = \chi N(t) \left[1 - \left(\frac{N(t)}{N_\infty}\right)^\theta\right], \quad (32)$$

completed with the initial value

$$N(t_0) = N_0.$$

In the model, $N_{\text{base}} + N_0$ corresponds to the value $\text{CR}(t_0)$ of the cumulative number of cases at time $t = t_0$. The parameter $N_\infty + N_{\text{base}}$ is the maximal value of the cumulative reported cases after the time $t = t_0$. $\chi > 0$ is a Malthusian growth parameter, and θ regulates the speed at which $\text{CR}(t)$ increases to $N_\infty + N_{\text{base}}$.

Regularize the junction between the epidemic phases: Because the formula for $\tau(t)$ involves derivatives of the phenomenological model regularizing $\text{CR}(t)$ (see equations (8)), we need to connect the phenomenological models of the different phases (epidemic and endemic) as smoothly as possible. Let t_0, \dots, t_n denote the $n + 1$ breaking points of the model, that is, the times at which there is a transition between one phase and the next one. We let $\widetilde{\text{CR}}(t)$ be the global model obtained by placing the phenomenological models of the different phases side by side.

More precisely, $\widetilde{\text{CR}}(t)$ is defined by (30) during an epidemic phase $[t_i, t_{i+1}]$, or during the initial phase $(-\infty, t_0]$ or the last phase $[t_n, +\infty)$. During an endemic phase, $\widetilde{\text{CR}}(t)$ is defined by (29). The parameters are chosen so that the resulting global model $\widetilde{\text{CR}}$ is continuous. We define the regularized model by using the convolution formula:

$$\text{CR}(t) = \int_{-\infty}^{+\infty} \mathcal{G}(t-s) \times \widetilde{\text{CR}}(s) ds = (\mathcal{G} * \widetilde{\text{CR}})(t), \quad (33)$$

where

$$\mathcal{G}(t) := \frac{1}{\sigma\sqrt{2\pi}} e^{-\frac{t^2}{2\sigma^2}}$$

is the Gaussian function with mean 0 and variance σ^2 . The parameter σ controls the trade-off between smoothness and precision: increasing σ reduces the variations in $\text{CR}(t)$ and reducing σ reduces the distance between $\text{CR}(t)$ and $\widetilde{\text{CR}}(t)$. In any case the resulting function $\text{CR}(t)$ is very smooth (as well as its derivatives) and close to the original model $\widetilde{\text{CR}}(t)$ when σ is not too large. Here, we fix

$$\sigma = 7 \text{ days.}$$

Numerically, we will need to compute some $t \rightarrow \text{CR}(t)$ derivatives. Therefore it is convenient to take advantage of the convolution (33) and deduce that

$$\frac{d^n \text{CR}(t)}{dt^n} = \int_{-\infty}^{+\infty} \frac{d^n \mathcal{G}(t-s)}{dt^n} \times \widetilde{\text{CR}}(s) ds, \quad (34)$$

for $n = 1, 2, 3$.

7.2. Phenomenological Model apply to France

Figures 19-20 below is taken from [51]. In Figure 19, we present the best fit of our phenomenological model for the cumulative reported case data of COVID-19 epidemic in France. The yellow regions correspond to the endemic phases and the blue regions correspond to the epidemic phases. Here we consider the two epidemic waves for France, and the chosen period, as well as the parameters values for each period.

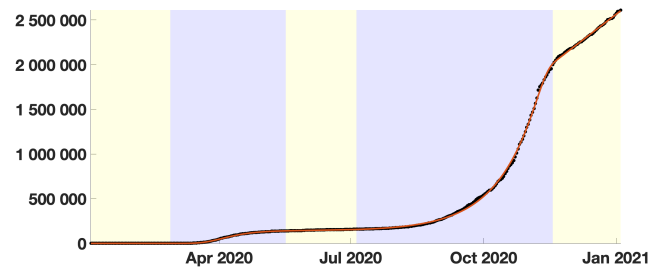


Figure 19. The red curve corresponds to the phenomenological model and the black dots correspond to the cumulative number of reported cases in France.

Figure 20 shows the corresponding daily number of new reported cases data (black dots) and the first derivative of our phenomenological model (red curve).

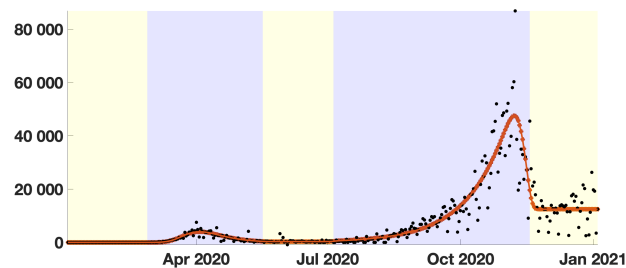


Figure 20. The red curve corresponds to the phenomenological model and the black dots correspond to the daily number of reported cases in France.

7.3. Phenomenological Model apply to several countries

Our method to regularize the data was applied to the eight geographic areas. The resulting curves are presented in Figure 21. The blue background color regions correspond to epidemic phases and the yellow background color regions to endemic phases. We added a plot of the daily number of cases (black dots) and the derivative of the regularized model for comparison, even though the daily number of cases is not used in the fitting procedure. The figures generally show an excellent agreement between the time series of reported cases (top row, black dots) and the regularized model (top row, blue curve). The match between the daily number of cases (bottom row, black dots) and the derivative of the regularized model (bottom row, blue curve) is also excellent, even though it is not a part of the optimization process. Of course, we lose some information, like the extreme values (“peaks”) of the daily number of cases. This is because we focus on an averaged value of the number of cases. More information could be retrieved by statistically studying the variation around the phenomenological model. However, we leave such a study for future work. The relative error between the regularized curve and the data may be relatively high at the beginning of the epidemic because of the stochastic nature of the infection process and the small number of infected individuals but quickly drops below 1% (see the supplementary material in [52] for more details).

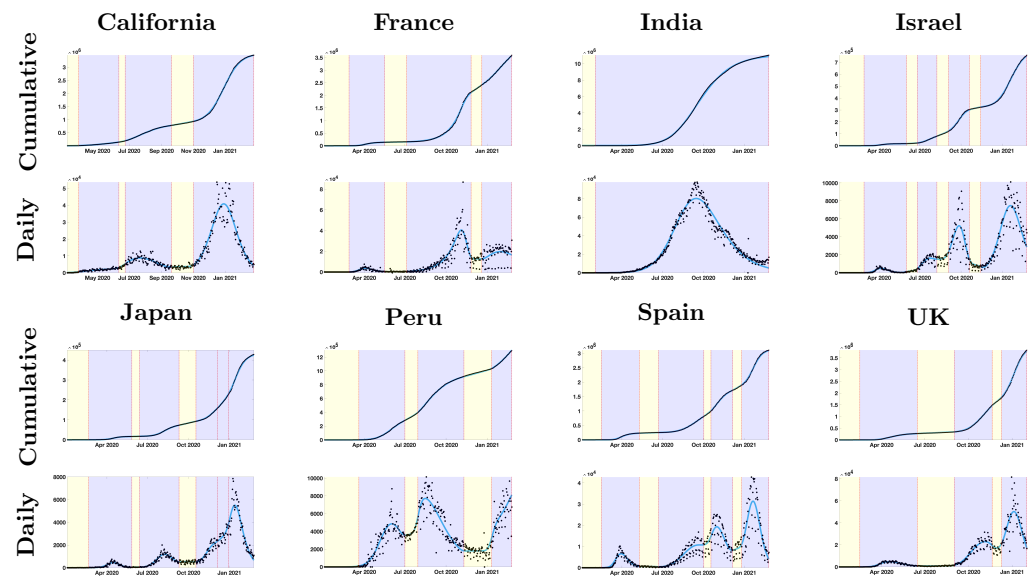


Figure 21. In the top rows, we plot the cumulative number of reported cases (black dots) and the best fit of the phenomenological model (blue curve). In the bottom rows, we plot the daily number of reported cases (black dots) and the first derivative of the phenomenological model (blue curve). This figure is taken from [52].

7.4. Earlier results about transmission rate reconstructed from the data

This problem has already been considered in several articles. In the early 70s, London and Yorke [34,35] discussed the time dependent rate of transmission in the context of measles, chickenpox and mumps. Motivated by applications to the data for COVID-19 in [53] the authors also obtained some new results about reconstructing the rate of transmission.

7.5. Instantaneous reproduction number

We use the formula (8) to compute the transmission rate, and we consider the **instantaneous reproduction number**

$$\mathbf{R}_e(t) = \tau(t)\mathbf{S}(t)/\nu,$$

and the **quasi-instantaneous reproduction number**

$$\mathbf{R}_e^0(t) = \tau(t)\mathbf{S}_0/\nu,$$

We compare the above indicators with $\mathbf{R}_e^C(t)$ the classical notion of **instantaneous reproduction number** [54–56].

Remark 13. The standard method to compute $\mathbf{R}_e^C(t)$ (see [54–56]) proposes another form of regularization of the data, which consists of computing the instant of contamination backward in time. This instant is random and follows a standard exponential law.

7.6. Results

In Figure 22, our analysis allows us to compute the transmission rate $\tau(t)$. We use this transmission rate to calculate two different indicators of the epidemiological dynamics for each geographic area, the instantaneous reproduction number and the quasi-instantaneous reproduction number. Both coincide with the basic reproduction number R_0 on the first day of the epidemic. The instantaneous reproduction number at time t , $R_e(t)$, is the basic reproduction number corresponding to an epidemic starting at time t with a constant transmission rate equal to $\tau(t)$ and with an initial population of susceptibles composed of $S(t)$ individuals (the number of susceptible individuals remaining in the population).

The quasi-instantaneous reproduction number at time t , $R_e^0(t)$, is the basic reproduction number corresponding to an epidemic starting at time t with a constant transmission rate equal to $\tau(t)$ and with an initial population of susceptibles composed of S_0 individuals (the number of susceptible individuals at the start of the epidemic). The two indicators are represented for each geographic area in the top row of Figure 22 (black curve: instantaneous reproduction number; green curve: quasi-instantaneous reproduction number).

One interpretation for $R_e(t)$ and another for $R_e^0(t)$. The instantaneous reproduction number indicates if, given the current state of the population, the epidemic tends to persist or die out in the long term (note that our model assumes that recovered individuals are perfectly immunized). The quasi-instantaneous reproduction number indicates if the epidemic tends to persist or die out in the long term, provided the number of susceptible is the total population. In other words, we forget about the immunity already obtained by recovered individuals. Also, it is directly proportional to the transmission rate and therefore allows monitoring of its changes. Note that the value of $R_e^0(t)$ changed drastically between epidemic phases, revealing that $\tau(t)$ is far from constant. In any case, the difference between the two values starts to be visible in the figures one year after the start of the epidemic.

We also computed the reproduction number using the method described in [55], which we denoted $R_e^C(t)$. The precise implementation is described in the supplementary material in [52]. It is plotted in the bottom row of Figure 22 (green curve), along with the instantaneous reproduction number $R_e(t)$ (green curve).

Remark 14. In the bottom of Figure 22, we compare the instantaneous reproduction numbers obtained by our method in black and the classical method in [55] in green. We observe that the two approaches are not the same at the beginning. This is because the method of [55] does not consider the initial values I_0 and E_0 while we do. Indeed the method of [55] assumes that I_0 and E_0 are close to 0 at the beginning when it is viewed as a Volterra equation reformulation of the Bernoulli–Kermack–McKendrick model with the age of infection. On the other hand, our method does not require such an assumption since it provides a way to compute the initial states I_0 and E_0 .

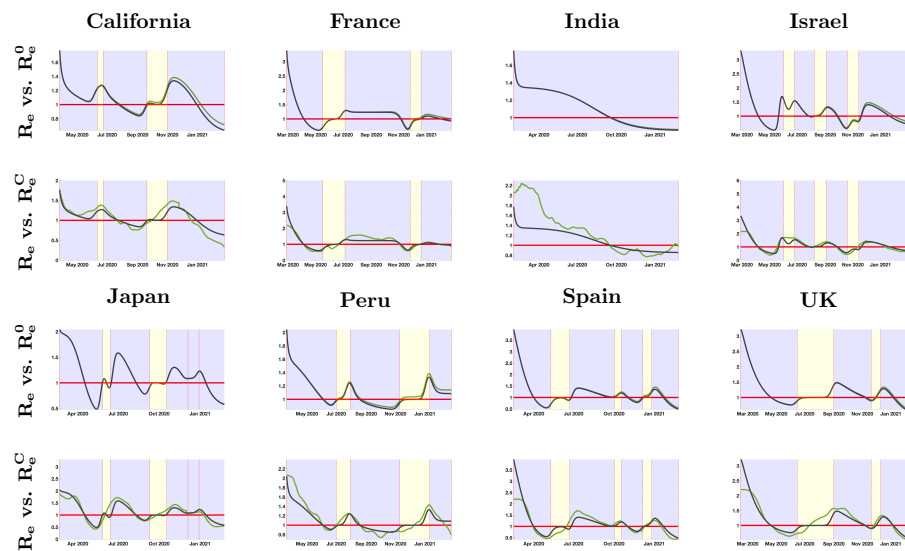


Figure 22. In the top rows, we plot the instantaneous reproduction number $R_e(t)$ (in black) and the quasi instantaneous reproduction number $R_e^0(t)$ (in green). In the bottom rows, we plot the instantaneous reproduction number $R_e(t)$ (in black) and the one obtained by the standard method [54,55] $R_e^C(t)$ (in green). This figure is taken from [52].

It is essential to “regularize” the data to obtain a comprehensive outcome from SIR epidemic models. In general, the rate of transmission in the SIR model (applying identification methods) is not very noisy and meaningless. For example, at the beginning of the first epidemic wave, the transmission rate should be decreasing since peoples tend to have less and less contact while to epidemic growth. The standard regularization methods (like, for example, the rolling weekly average method) have been tested for COVID-19 data in [8]. The outcome in terms of transmission rate is very noisy and even negative transmission (which is impossible). Regularizing the data is not an easy task, and the method used is very important in order to obtain a meaningful outcome for the models. Here, we tried several approaches to link an epidemic phase to the next endemic phase. So far, this regularization procedure is the best one.

Figure 23 illustrates why we need a phenomenological model to regularize the data. On the left-hand side, we observe the $\tau(t)$ becomes negative almost immediately. Therefore, without regularization, the fit may not make sense.

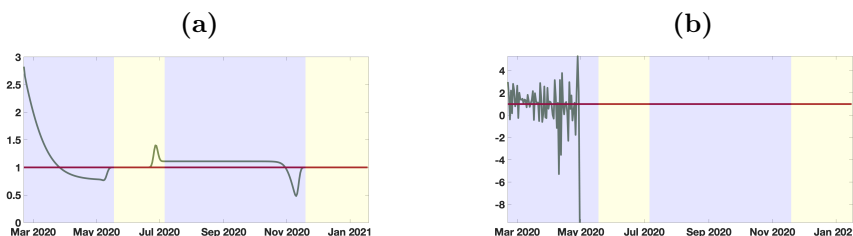


Figure 23. In this figure, we plot the instantaneous R_0 . On the left-hand side, we use our smoothing method (with Bernoulli-Verhulst model (endemic) line (endemic) together with a convolution with a Gaussian). On the right-hand side, we use the original cumulative data and our algorithm to fit the cumulative number of cases.

7.7. Consequences of the results

In Figure 22, we saw that the population of susceptible patients is almost unchanged after the epidemic passed. Therefore, the system behaves almost like the non-autonomous system

$$I'(t) = \tau(t)S_0I(t) - \nu I(t), \forall t \geq t_0, \text{ and } I(t_0) = I_0,$$

This means that $I(t)$ depends linearly on I_0 . That is, if we multiply I_0 by some number, the result $I(t)$ will be multiply by the same number.

Figure 24 shows two things. The initial number of infected is crucial when we try to predict the number of infected. The average daily number of cases during the endemic phases have strong impact on the amplitude of the next epidemic waves [51].

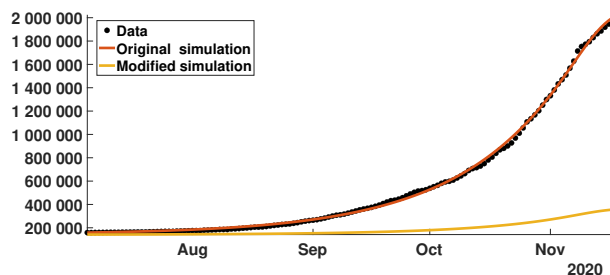


Figure 24. We start the simulation at time $t_0 = \text{July } 5, 2020$ with the initial value $I_0 = \frac{CR'(t_2)}{\nu f}$ for red curve and with $I_0 = 0.41 \frac{CR'(t_2)}{\nu f}$ for yellow curve).

In this section, we obtained a model that cover the changes of regimen (from endemic to epidemic and conversely). Moreover the detection of the changes of regimen between epidemic wave and endemic period is still difficult to detect. An attempt to study this question can be found in [57].

8. Exponential phase with more compartments

8.1. A model with transmission from the unreported infectious

We consider a model with unreported infection individuals.

$$\begin{cases} S'(t) = -\tau(t)S(t)(I(t) + U(t)), \\ I'(t) = \tau(t)S(t)(I(t) + U(t)) - \nu I(t), \\ U'(t) = \nu(1 - f)I(t) - \eta U(t), \end{cases} \quad (35)$$

for $t \geq t_0$, and with initial distribution

$$S(t_0) = S_0, I(t_0) = I_0, \text{ and } U(t_0) = U_0. \quad (36)$$

The epidemic model associated with the flowchart in Figure 25 applies to influenza outbreaks in [58], hepatitis A outbreaks in [59], and COVID-19 in [9].

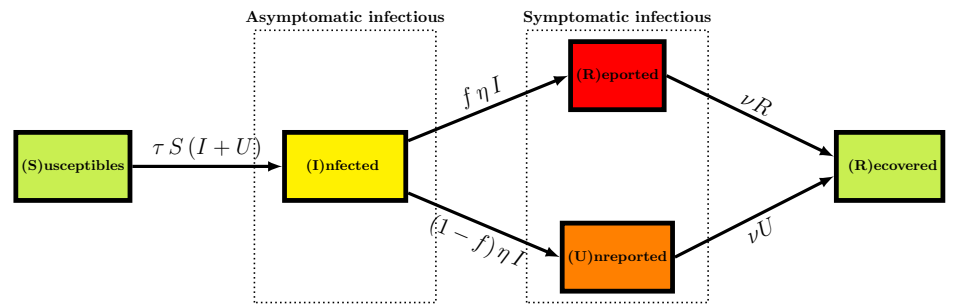


Figure 25. Flowchart.

8.2. The exponential phase approximation

We assume that $S(t)$ is constant, and equal to S_0 , and $\tau(t)$ remains constant equal to $\tau_0 = \tau(t_0)$. The consider for example the case of a single age group, we obtain the following model which was first considered for COVID-19

$$\begin{cases} I'(t) = \tau S_0(I(t) + U(t)) - \nu I(t), \\ U'(t) = \nu(1 - f)I(t) - \eta U(t), \end{cases} \quad (37)$$

for $t \geq t_0$, and with initial distribution

$$I(t_0) = I_0, \text{ and } U(t_0) = U_0. \quad (38)$$

We can reformulate this system using a matrix formulation

$$\begin{pmatrix} I'(t) \\ U'(t) \end{pmatrix} = A \begin{pmatrix} I(t) \\ U(t) \end{pmatrix}, \forall t \in [t_0, t_1],$$

where

$$A = \begin{pmatrix} \tau S_0 - \nu & \tau S_0 \\ \nu(1 - f) & -\eta \end{pmatrix}.$$

Then the matrix A is **irreducible** if and only if

$$\nu(1 - f) > 0 \text{ and } \tau S_0 > 0.$$

Remember the model (37) to connect the data and the epidemic model

$$CR'(t) = f\nu I(t), \text{ for } t \geq t_0.$$

Consider the **exponential phase of the epidemic**. That is,

$$CR'(t) = \chi_1\chi_2 e^{\chi_2 t}, \forall t \in [t_0, \tau + t_0],$$

for some $\tau > 0$. Combining the two previous equations, we obtain

$$f\nu I(t) = \chi_1 e^{\chi_2(t-t_0)}, \forall t \in [t_0, \tau + t_0],$$

Remember that χ_1 and χ_2 are computed by using the data. More precisely, these parameters are obtained by fitting $t \rightarrow \chi_1 e^{\chi_2 t} - \chi_3$ to the cumulative number of cases data during a period of time $[t_0, \tau + t_0]$. 564
565
566

We can rewrite $f\nu I(t) = \chi_1 e^{\chi_2 t}$ by using an inner product

$$\left\langle y_0, \begin{pmatrix} I(t) \\ U(t) \end{pmatrix} \right\rangle = \chi_1 e^{\chi_2 t}, \text{ with } y_0 = \begin{pmatrix} \nu f \\ 0 \end{pmatrix},$$

where $\langle \cdot, \cdot \rangle$ is the Euclidean inner product defined in dimension 2 as

$$\langle x, y \rangle = x_1 y_1 + x_2 y_2.$$

The following theorem is proved in Appendix A. 567

Theorem 15. *Let $\chi_1 > 0$, $\chi_2 > 0$, and $\tau > 0$. Let A be a n by n real matrix. Assume that the off-diagonal elements of A are non-negative, and A is irreducible. Assume that there exist two vectors $y_0 > 0$, and $x_0 > 0$ such that* 568
569
570

$$(Linear\ model) \quad \dot{x}(t) = Ax(t), \text{ and } x(0) = x_0,$$

satisfies

$$(Connection\ with\ the\ data) \quad \langle y_0, x(t) \rangle = \chi_1 e^{\chi_2 t}, \forall t \in [0, \tau],$$

where $\langle x, y \rangle$ is the Euclidean inner product. 571

Then χ_2 must be the dominant eigenvalue A (i.e., the one with the largest real part). Moreover, we can choose a vector $x_0 \gg 0$ (i.e., with all its components strictly positive), satisfying

$$Ax_0 = \chi_2 x_0.$$

Multiplying x_0 by a suitable positive constant, we obtain $\langle y_0, x_0 \rangle = \chi_1$, and we obtain 572

$$\langle y_0, x(t) \rangle = \chi_1 e^{\chi_2 t}, \forall t \in [0, \tau].$$

Returning back to the example of epidemic model with unreported cases, we must find $I(0) > 0$ and $U(0) > 0$ such that

$$\begin{pmatrix} \tau S_0 - \nu & \tau S_0 \\ \nu(1-f) & -\eta \end{pmatrix} \begin{pmatrix} I(0) \\ U(0) \end{pmatrix} = \chi_2 \begin{pmatrix} I(0) \\ U(0) \end{pmatrix}.$$

After a few computations (see the supplementary in Liu et al. [9]), we obtain 573

$$\tau = \frac{\chi_2 + \nu}{S_0} \frac{\eta + \chi_2}{\nu(1-f) + \eta + \chi_2}, \quad (39)$$

and

$$U_0 = \frac{\nu(1-f)}{\eta + \chi_2} I_0 = \frac{(1-f)\nu}{\eta + \chi_2} I_0. \quad (40)$$

Remark 16. Let $\chi_1 > 0$, $\chi_2 > 0$, $\phi_1 > 0$, $\phi_2 > 0$, and $\tau > 0$. Assume that $x_0 > 0$, $y_0 > 0$ and $z_0 > 0$ satisfy

$$\dot{x}(t) = Ax(t), \text{ and } x(0) = x_0,$$

and

$$\begin{aligned} \langle y_0, x(t) \rangle &= \chi_1 e^{\chi_2 t}, \forall t \in [0, \tau], \\ \langle z_0, x(t) \rangle &= \phi_1 e^{\phi_2 t}, \forall t \in [0, \tau]. \end{aligned}$$

If $\chi_2 \neq \phi_2$ the matrix A must be reducible. That is, up to a re-indexation of the components of $x(t)$, the matrix A reads as

$$A = \begin{pmatrix} A_{11} & 0 \\ A_{21} & A_{22} \end{pmatrix}$$

where A_{ij} are block matrices. The matrix A presents a weak coupling between the last block's components and the first block's components.

8.3. Uncertainty due to the period chosen to fit the data

The principle of our method is the following. By using an exponential best fit method we obtain a best fit of (6) to the data over a time $[t_1, t_2]$ and we derive the parameters χ_1 and χ_2 . The values of I_0 , U_0 , and τ_0 are obtained by using (7), (36) and (37). Next, we use

$$\tau(t) = \tau_0 e^{-\mu(t-N)^+},$$

we fix N (first day of public intervention) to some value and we obtain μ by trying to get the best fit to the data.

In the method the uncertainty in our prediction is due to the fact that several sets of parameters (t_1, t_2, N, f) may give a good fit to the data. As a consequence, at the early stage of the epidemics (in particular before the turning point) the outcome of our method can be very different from one set of parameters to another. We try to solve this uncertainty problem by using several choices of the period to fit an exponential growth of the data to determine χ_1 and χ_2 and several choices for the first day of intervention N . So in this section, we vary the time interval $[t_1, t_2]$, during which we use the data to obtain χ_1 and χ_2 by using an exponential fit. In the simulations below, the first day t_1 and the last day t_2 vary such that

$$\text{Earliest day} \leq t_1 \leq t_2 \leq \text{Latest day}.$$

We also vary the first day of public intervention:

$$\text{Earliest first day of intervention} \leq N \leq \text{Latest first day of intervention}.$$

We vary f between 0.1 to 0.9. For each $(t_1, t_2, \nu, f, \eta, \mu, N)$ we evaluate μ to obtain the best fit of the model to the data. We use the mean absolute deviation as the distance to data to evaluate the best fit to the data. We obtain a large number of best fit depending on $(t_1, t_2, \nu, f, \eta, \mu, N)$ and we plot smallest mean absolute deviation MAD_{\min} . Then we plot all the best fit graphs with mean absolute deviation between MAD_{\min} and $\text{MAD}_{\min} + 40$.

The figure below is taken from Liu et al. [60].

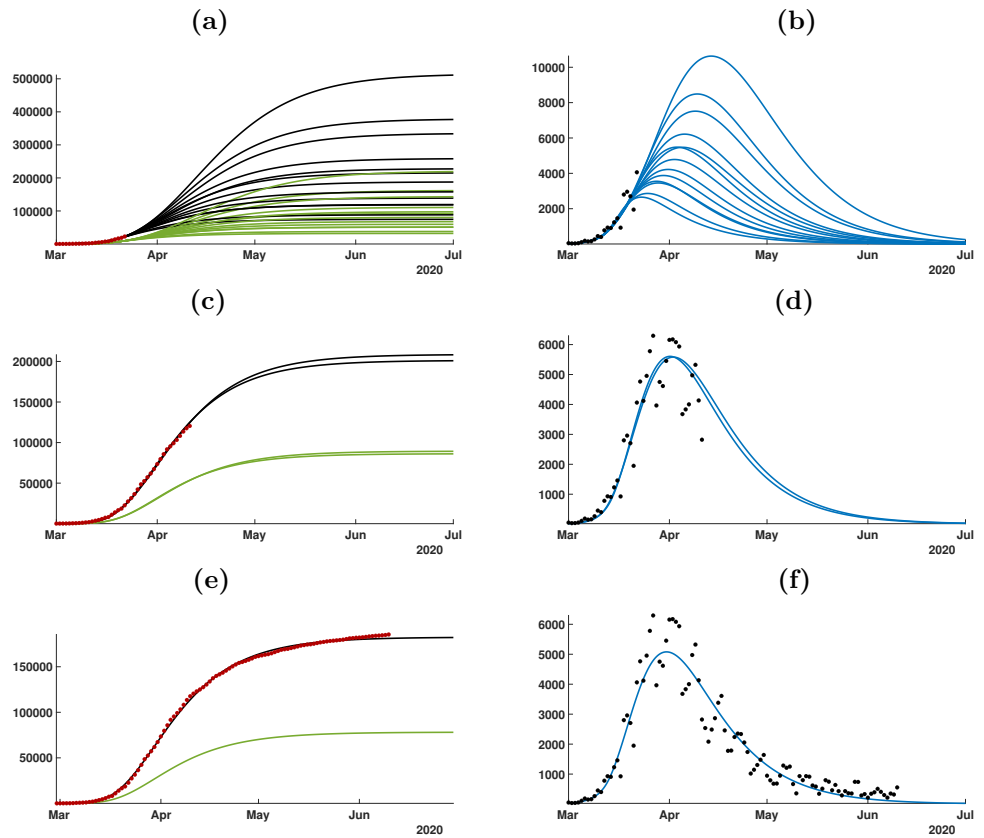


Figure 26. In this figure, we consider the data for Germany. We plot the cumulative number of cases of the left hand side and the daily number of cases on the right hand side. In (a) and (b) we use the data until March 22. In (c) and (d) we use the data until April 11. (e) and (f) we use the data until June 10.

9. Modeling COVID-19 epidemic with age groups

This section considers an epidemic whenever the population is divided into age groups. Here, age means the chronological age, which is nothing but the time since birth.

9.1. Epidemic model with age groups

The epidemic model with age structure and unreported cases reads as follows, for each $t \geq t_0$,

$$\begin{cases} S'_1(t) = -\tau_1 S_1(t) \left[\phi_{11} \frac{I_1(t) + U_1(t)}{N_1} + \dots + \phi_{1n} \frac{I_n(t) + U_n(t)}{N_n} \right], \\ \vdots \\ S'_n(t) = -\tau_n S_n(t) \left[\phi_{n1} \frac{I_1(t) + U_1(t)}{N_1} + \dots + \phi_{nn} \frac{I_n(t) + U_n(t)}{N_n} \right], \\ \vdots \\ I'_1(t) = \tau_1 S_1(t) \left[\phi_{11} \frac{I_1(t) + U_1(t)}{N_1} + \dots + \phi_{1n} \frac{I_n(t) + U_n(t)}{N_n} \right] - \nu I_1(t), \\ \vdots \\ I'_n(t) = \tau_n S_n(t) \left[\phi_{n1} \frac{I_1(t) + U_1(t)}{N_1} + \dots + \phi_{nn} \frac{I_n(t) + U_n(t)}{N_n} \right] - \nu I_n(t), \end{cases}$$

and

$$\begin{cases} U'_1(t) = \nu_2^1 I_1(t) - \eta U_1(t), \\ \vdots \\ U'_n(t) = \nu_2^n I_n(t) - \eta U_n(t), \end{cases}$$

586

587

588

589

with the initial values

$$S_i(t_0) = S_i^0, I_i(t_0) = I_i^0, \text{ and } U_i(t_0) = U_i^0, \forall i = 1, \dots, n.$$

9.2. Cumulative reported cases with age structure in Japan

We first choose two days d_1 and d_2 between which each cumulative age group grows like an exponential. By fitting the cumulative age classes $[0, 10[, [10, 20[, \dots$ and $[90, 100[$ between d_1 and d_2 , for each age class $j = 1, \dots, 10$ we can find χ_1^j, χ_2^j and χ_3^j

$$CR_j^{data}(t) \simeq \chi_1^j e^{\chi_2^j t} - \chi_3^j.$$

We obtain

$$\begin{cases} CR_1(t) = \chi_1^1 e^{\chi_2^1 t} - \chi_3^1, \\ \vdots \\ CR_n(t) = \chi_1^n e^{\chi_2^n t} - \chi_3^n, \end{cases} \tag{41}$$

where

$$\chi_j^i \geq 0, \forall i = 1, \dots, n, \forall j = 1, 2, 3.$$

In Figures 27-28, the growth rate of the exponential fit depends on the age group [61]. In Figures 27-28, we see the similarity of dynamical behavior at the two extreme age groups $[0, 20]$ and $[70, 100]$.

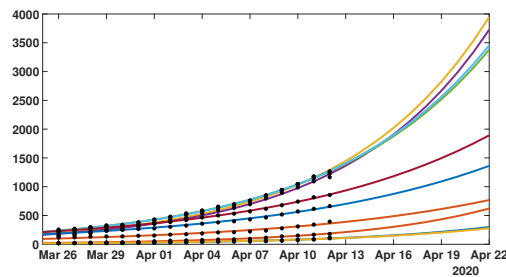


Figure 27. In this figure, we plot an exponential fit to the cumulative data for each age groups $[0, 10[, [10, 20[, \dots$ and $[90, 100[$ in Japan.

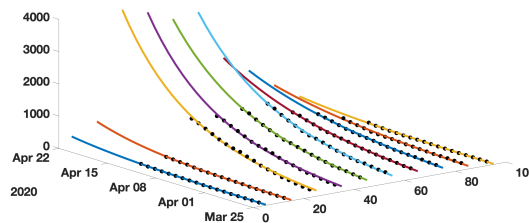


Figure 28. In this figure, we plot an exponential fit to the cumulative data for each age groups $[0, 10[, [10, 20[, \dots$ and $[90, 100[$ in Japan.

9.3. Method to Fit of the Age Structured Model to the Data

By assuming that the number of susceptible individuals remains constant we have for each $t \geq t_0$,

$$\begin{cases} I_1'(t) = \tau_1 S_1 \left[\phi_{11} \frac{I_1(t) + U_1(t)}{N_1} + \dots + \phi_{1n} \frac{I_n(t) + U_n(t)}{N_n} \right] - \nu I_1(t), \\ \vdots \\ I_n'(t) = \tau_n S_n \left[\phi_{n1} \frac{I_1(t) + U_1(t)}{N_1} + \dots + \phi_{nn} \frac{I_n(t) + U_n(t)}{N_n} \right] - \nu I_n(t), \end{cases}$$

and

$$\begin{cases} U_1'(t) = \nu_2^1 I_1(t) - \eta U_1(t), \\ \vdots \\ U_n'(t) = \nu_2^n I_n(t) - \eta U_n(t), \end{cases} \quad (42)$$

with the initial values

$$I_i(t_0) = I_i^0, \text{ and } U_i(t_0) = U_i^0, \forall i = 1, \dots, n.$$

9.4. Rate of contact

The values in Figure 29 describe the contact rates between age groups. The values used are computed from the values obtained in [62].

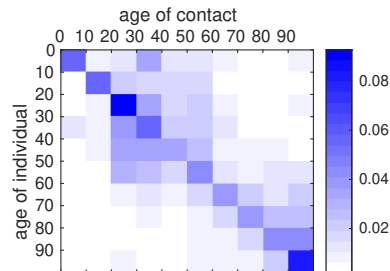


Figure 29. For each age class in the y-axis we plot the rate of contacts between one individual of this age class and another individual of the age class indicated on the x-axis. The figure represents the rate of contacts before the start of public measures (April 11).

We assume that

$$\begin{cases} CR_1(t)' = \nu_1^1 I_1(t), \\ \vdots \\ CR_n(t)' = \nu_1^n I_n(t), \end{cases}$$

where

$$\nu_1^i = \nu f_i, \text{ and } \nu_2^i = \nu(1 - f_i), \forall i = 1, \dots, n.$$

Therefore, we obtain

$$I_j(t) = I_j^* e^{\chi_2^j t},$$

where

$$I_j^* := \frac{\chi_1^j \chi_2^j}{\nu_1^j}.$$

If we assume that the $U_j(t)$ have the following form

$$U_j(t) = U_j^* e^{\chi_2^j t},$$

then by substituting in (42) we obtain

$$U_j^* = \frac{\nu_2^j I_j^*}{\eta + \chi_2^j}.$$

The cumulative number of unreported cases $CU_j(t)$ is computed as

$$CU_j(t)' = \nu_2^j I_j(t),$$

and we used the following initial condition:

$$CU_j(0) = CU_j^* = \int_{-\infty}^0 \nu_2^j I_j^* e^{\chi_2^j s} ds = \frac{\nu_2^j I_j^*}{\chi_2^j}.$$

We define the error between the data and the model as follows

$$\begin{cases} I_1'(t) = \tau_1 S_1 \left[\phi_{11} \frac{I_1(t) + U_1(t)}{N_1} + \dots + \phi_{1n} \frac{I_n(t) + U_n(t)}{N_n} \right] - \nu I_1(t) + \varepsilon_1(t), \\ \vdots \\ I_n'(t) = \tau_n S_n \left[\phi_{n1} \frac{I_1(t) + U_1(t)}{N_1} + \dots + \phi_{nn} \frac{I_n(t) + U_n(t)}{N_n} \right] - \nu I_n(t) + \varepsilon_n(t), \end{cases}$$

or equivalently

$$\begin{cases} \varepsilon_1(t) = (\chi_2^1 + \nu) I_1^* e^{\chi_2^1 t} - \tau_1 S_1 \left[\phi_{11} \frac{I_1^* + U_1^*}{N_1} e^{\chi_2^1 t} + \dots + \phi_{1n} \frac{I_n^* + U_n^*}{N_n} e^{\chi_2^1 t} \right], \\ \vdots \\ \varepsilon_n(t) = (\chi_2^n + \nu) I_n^* e^{\chi_2^n t} - \tau_n S_n \left[\phi_{n1} \frac{I_1^* + U_1^*}{N_1} e^{\chi_2^n t} + \dots + \phi_{nn} \frac{I_n^* + U_n^*}{N_n} e^{\chi_2^n t} \right]. \end{cases}$$

Lemma 17. Assume that the matrix ϕ be fixed. If we consider the errors $\varepsilon_1^\tau(t), \dots, \varepsilon_n^\tau(t)$ as a function of τ , then we can a unique value $\tau^* = (\tau_1^*, \dots, \tau_n^*)$ which minimizes that L^2 norm of the errors. That

$$\sum_{j=1, \dots, n} \int_{d_1}^{d_2} \varepsilon_j^{\tau^*}(t)^2 dt = \min_{\tau \in \mathbb{R}^n} \sum_{j=1, \dots, n} \int_{d_1}^{d_2} \varepsilon_j^\tau(t)^2 dt.$$

Moreover,

$$\tau_j^* = \frac{\int_{d_1}^{d_2} K_j(t) H_j(t) dt}{\int_{d_1}^{d_2} H_j(t)^2 dt},$$

with

$$K_j(t) := (\chi_2^j + \nu) I_j^* e^{\chi_2^j t}, \forall j = 1, \dots, n,$$

and

$$H_j(t) := S_j \left[\phi_{j1} \frac{I_1^* + U_1^*}{N_1} e^{\chi_2^1 t} + \dots + \phi_{jn} \frac{I_n^* + U_n^*}{N_n} e^{\chi_2^n t} \right], \forall j = 1, \dots, n.$$

Proof. We look for the vector $\tau = (\tau_1, \dots, \tau_n)$ which minimizes of

$$\min_{\tau \in \mathbb{R}^n} \sum_{j=1, \dots, n} \int_{d_1}^{d_2} \varepsilon_j(t)^2 dt.$$

Define for each $j = 1, \dots, n$

$$K_j(t) := (\chi_2^j + \nu) I_j^* e^{\chi_2^j t}$$

and

$$H_j(t) := S_j \left[\phi_{j1} \frac{I_1^* + U_1^*}{N_1} e^{\chi_2^1 t} + \dots + \phi_{jn} \frac{I_n^* + U_n^*}{N_n} e^{\chi_2^n t} \right],$$

so that

$$\varepsilon_j(t) = K_j(t) - \tau_j H_j(t).$$

Hence for each $j = 1, \dots, n$

$$\int_{d_1}^{d_2} \varepsilon_j(t)^2 dt = \int_{d_1}^{d_2} K_j(t)^2 dt - 2\tau_j \int_{d_1}^{d_2} K_j(t) H_j(t) dt + \tau_j^2 \int_{d_1}^{d_2} H_j(t)^2 dt,$$

and the minimum of $\int_{d_1}^{d_2} \varepsilon_j(t)^2 dt$ is obtained for τ_j satisfying

$$0 = \frac{\partial}{\partial \tau_j} \int_{d_1}^{d_2} \varepsilon_j(t)^2 dt = -2 \int_{d_1}^{d_2} K_j(t) H_j(t) dt + 2\tau_j \int_{d_1}^{d_2} H_j(t)^2 dt$$

whenever

$$\tau_j = \frac{\int_{d_1}^{d_2} K_j(t) H_j(t) dt}{\int_{d_1}^{d_2} H_j(t)^2 dt}.$$

Under this condition, we obtain

$$\int_{d_1}^{d_2} \varepsilon_j(t)^2 dt = \int_{d_1}^{d_2} K_j(t)^2 dt - \tau_j^2 \int_{d_1}^{d_2} H_j(t)^2 dt.$$

□

600

Remark 18. *It does not seem possible to estimate the matrix of contact ϕ by using similar optimization method. Indeed, if we look for a matrix $\phi = (\phi_{ij})$ which minimizes*

$$\min_{\phi \in M_n(\mathbb{R})} \sum_{j=1, \dots, n} \int_{d_1}^{d_2} \varepsilon_j(t)^2 dt,$$

it turn out that

$$\sum_{j=1, \dots, n} \int_{d_1}^{d_2} \varepsilon_j(t)^2 dt = 0$$

whenever ϕ is diagonal. Therefore the optimum is reached for any diagonal matrix. Moreover by using similar considerations, if several χ_j^2 are equal, we can find a multiplicity of optima (possibly with ϕ not diagonal). This means that trying to optimize by using the matrix ϕ does not yield significant and reliable information.

601

602

603

604

In the Figure below, we present an example of application of our method to fit the Japanese data. We use the period going from 20 March to 15 April.

605

606

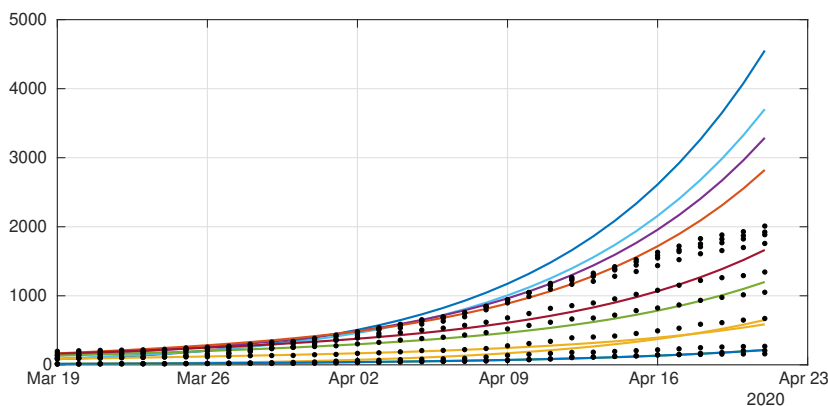


Figure 30. We plot a comparison between the model (without public intervention) and the age structured data from Japan (black dots).

In the Figure below, we present an example of application of our method to fit the Japanese data. We use the period going from 20 March to 15 April.

607
608

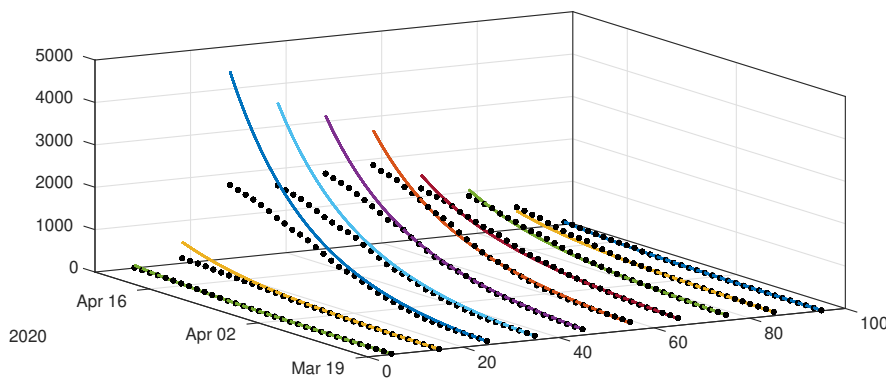


Figure 31. We plot a comparison between the model (without public intervention) and the age structured data from Japan (black dots).

10. A survey for COVID-19 mathematical modeling

609

During the COVID-19 pandemic, scientific workforces in different fields published COVID-19-related papers. The number of articles published increased considerably during this period. For example, on August 23, 2023, the WHO COVID-19 Research Database [63] contains 724288 full texts of articles concerning the COVID-19 outbreak. Consequently, providing an extensive review on the subject is hopeless. Here, we make some arbitrary choices that can always be discussed. Our main goal is to give extra references on the topics mentioned earlier and highlight topics not considered in the previous sections. Several articles have attempted to do systematic reviews on COVID-19. We refer to [64,65] for more results and a broader overview of the subject.

610
611
612
613
614
615
616
617
618

The idea of this survey was mostly to collect references from the Infectious Disease Outbreak webinar, which took place from 2020 to 2022 [66].

619
620

10.1. Medical survey

621

Mathematical models alone do not provide reliable information. In Figure 13, we show the divergence of the mathematical model from the data. It is therefore fundamental to bring medical results into the models.

622
623
624

It is therefore fundamental to integrate medical facts into mathematical models. We have tried throughout this text to explain how to make maximum use of the data either as input (test data) or as output (reported case data). But the dynamics of infection can

625
626
627

be understood much better by examining concrete case studies in hospitals. For example, modeling the dynamics of infectious clusters is crucial in preventing the spread of disease. We refer to [67–81] for more results and references.

The early development of an epidemic are very important, and an interesting retrospect of the first weeks of COVID-19 in China was presented by Zhao in [82].

10.2. Incubation, Infectiousness, and Recovery Period

The infectious dynamic has three phases:

- (i) The emission of the infectious agent, which depends on its concentration during its expulsion (remotely by air transportation or directly by secretion contact) from the contagious person;
- (ii) Transmission of the infectious agent (through an intermediate fluid or on a contact surface);
- (iii) The reception of the infectious agent by a future host who becomes infected and whose symptomatology and secondary emission capacities will depend on the infectious agent's pathogenic nature and the host's immune defenses.

These defenses are set up in two successive stages, corresponding to innate immunity, then to acquired immunity. It is, therefore, conceivable that the transmission capacity of an infectious person depends on the individual infection age. That is, the time since this person was infected. We refer to [3,83–89] for more results on the subject. In [90], we proposed a method to understand the average individual dynamic of infection by clusters data. When considering epidemic exponential phase data, a time series approach is proposed in [11]. We refer to [91] for more results on the subject.

10.3. Data

An essential aspect of epidemics outbreaks is understanding the biases in the data. That is the different causes, such as unreported case data, tests, false positive PRC tests, and other factors that may bias our understanding of the data. Clusters of infected also provide another kind of data that may give another angle to examine the same problem. We should also mention the data provided by the wasted water that offers a helpful complement to the existing reported case data.

10.3.1. Contact tracing

Contact tracing has been the main tool of public health authorities, for example, in South Korea when the COVID-19 pandemic started. In France, a dedicated digital tool called Stop-Covid has been developed. In [92], authors estimate that this digital approach was adopted not because digital solutions (to contact tracing) are superior to traditional ones but by default due to alienation and lack of interdisciplinary cooperation, which could be due to the fact that contact tracing is balancing personal privacy and public health, causing significant biases in classical inquiries with questionnaires [93]. We refer to [91–104] for more results on the subject.

10.3.2. Testing data

A mathematical model to understand the bias in PCR tests was proposed first by [105,106]. Diagnostic tests, particularly the PCR test, have been of considerable importance in most countries' follow-up of new cases. We refer [107–113]. Mathematical models, including testing data as an input of the model, were proposed by [5,114].

10.3.3. Unreported and uncertainty in the number of reported case data

The origin of unreported cases of COVID-19 is multiple. It may be due to

- (i) a poor organization of the reporting system by the medical profession or recording by the administrative staff (especially at weekends);
- (ii) The presence of asymptomatic cases;

- (iii) The non-consultation and/or the non-taking of medication in the symptomatic case, for reasons related to the patient or his entourage (presence of an intercurrent pathology or an existing chronic disease masking the symptoms, reasons financial, religious, philosophical, social, etc.).

We refer to [5,9,10,60,115–120] for more results on the subject.

10.3.4. Clusters

The detection and monitoring of clusters are difficult to achieve and the discovery of patient zero, in a given geographical area, is always a delicate challenge. Nevertheless, there are a number of studies regarding this problem. We refer to [121–128] for more results on the subject.

10.3.5. More phenomenological model to fit the data

Since Daniel Bernoulli's classic primordial model [39–42], a number of phenomenological models have emerged, such as that of Richards that Ma cited [129] just before the beginning of Covid-19 outbreak. The COVID-19 pandemic was an opportunity to recall this princeps work and to propose new approaches along the same lines, namely minimal modeling integrating the basic mechanisms of infectious transmission. We refer to [51,129–136] for more results and references on the subject.

10.3.6. Wasted water data

The French national Obepine project has shown the value of monitoring the COVID-19 pandemic in wastewater, where the concentration of viral RNA fragments can serve as an early indicator of the onset of new waves of cases. An Italian study (Gragnani et al.) has even suggested that SARS-Cov-2 RNA was present in wastewater from Milan, Turin (December 18, 2019) and Bologna (January 29, 2020) long before the first Italian case was described (February 20 2020). We refer to [137–144] for more results on the subject.

10.3.7. Discrete and random modeling

Some modeling approaches are discrete and play with daily data. The equations of the contagion dynamics can be of two types:

- (i) They can be difference equations modeled on the differential equations of the continuous SIR model;
- (ii) or they can be stochastic in nature, with generally additive Gaussian noise in the second member.

They generally lend themselves well to the statistical estimation of their parameters from the data. We refer to [145–148] for more results and references on the subject.

10.3.8. Time series and wavelet approaches

If we consider the data recorded on the size of the different sub-populations involved in the contagion process (susceptible, infected, cured, immune, etc.), a possible approach is that of the signal theory, with its classical methods data processing (time series, Fourier transformation, wavelet transformation, etc.). This approach is generally an excellent introduction to the implementation of prediction methods. We refer to [11,130,149–152] for more results and references on the subject.

10.3.9. Transmission estimation and spatial modeling

Estimating the transmission parameter and studying its spatio-temporal variations is fundamental because it conditions the epidemic waves' location, shape, and duration. The spatial heterogeneity of this parameter, often due to geo-climatic (such as temperature) and/or demographic (such as susceptible population density), are crucial factors in the existence of natural barriers to the spread of a pandemic. We refer to [153–156] for more results and references on the subject.

The generation time characterizes the speed at which infections occur and differs in different populations and between SARS-CoV-2 variants. This is a key epidemiological factor that was estimated for SARS-CoV-2 in [96,157,158].

10.3.10. Forecasting methods

The prediction of epidemics is one of the major objectives of modeling. It can be carried out by the continuation, in time and space, of the solutions of the spatio-temporal equations of the chosen model or the extrapolation of a statistical description of the evolution of the observed variables. We refer to [53,60,159–161] for more results and references on the subject.

10.4. *SIR like models*

Since 2020, many articles have appeared on using the SIR model in modeling the COVID-19 outbreak. After [9], several SIR with the symptomatic and asymptomatic compartment, in order to model reported and unreported patients mechanisms. Several article along this line were published [162–166].

The major default of this study is the fact that they use a transmission rate constant in time. This assumption allows, for example, [164] to estimate the fraction of unreported patients. As explained in section 6, the transmission rate must be time-dependent. In [8], we proved that it is hopeless to estimate the fraction of unreported patients since we can get the exact same fit to the data for a large interval of values of this parameter. Several groups realized that time-dependent transmission rate in an important issue in such a problems [8,10,18–20,51–53,60,120].

During COVID-19 pandemic, models progressively complexified to become SIAURDV models, incorporating explicitly as ODE variables the numbers of asymptomatic (A), non-reported (U), vaccinated (V), and deceased (D) patients. We refer to [167–172] for more results and references on the subject.

10.4.1. Multigroups or multiscale models

The notion of multi-group and multi-scale appeared when the COVID-19 outbreak appeared, with specific dynamics in several geographical regions of different scales and, in one area, in several distinct groups (demographic, ethnic, economic, religious, social, etc.). We refer to [166,173–178] for more results and references on the subject.

10.4.2. Model with unreported or asymptomatic compartment

Modeling the mechanisms of non-reporting of new cases or deaths due to an epidemic makes it possible to compensate for the bias coming from a partial observation of the infected, due to the existence of asymptomatic cases or a deficient administrative registration mechanism. We refer to [179–185] for more results and references on the subject.

10.5. *Connecting reported case data with SIR like model*

Very few studies considered that problem in the literature, while again, it is interesting to understand the bias induced by such a mechanism. For example, it would make sense to consider a model including a delay in reporting the data

$$CR'(t) = f\nu \int_0^\tau \gamma(s)I(t-s)ds$$

where $s \mapsto \gamma(s)$ is a non negative map. The quantity $\gamma(s)$ is the probability of reporting s units of time after the individual leaves the compartment I . This corresponds to patients showing symptoms. We deduce that we must have

$$\int_0^\tau \gamma(s)ds = 1.$$

Unfortunately, people have not considered this issue in the literature. The consequence of such a model for reported case data seems particularly important. We refer to [186–188] for more results and references on the subject.

10.6. *Re-infections, natural and hybrid immunity*

The risk of reinfection with the SARS-Cov2 virus comes from two factors:

- (i) One is due to the infectious agent and its mutagenic genius, modifying its contagiousness and pathogenicity;
- (ii) The other is due to the host, whose natural, innate, and acquired defenses by the adaptive immune system or artificially by vaccination prevent or stop the infection.

The modeling of these two facets of the reinfection process makes it possible to understand the mechanisms of eradication or, on the contrary, the continuation of a pandemic, thanks to or despite collective public health measures. We refer to [189–194] for more results and references on the subject.

10.7. *Mortality*

Mortality may appear as more robust data to be connected with epidemic models. The bias for report cases data will also exist for the number of reported dead patients. Again, the model to connect the data and the epidemic model might be more complex than a fraction of the recovered. Nevertheless, there is evidence of an increased risk of death in the event of co-infection. The mortality risk increases dramatically when a patient is infected with another severe disease. This question of co-infection with severe diseases with COVID-19 was studied in [195]. We refer to [196–203] for more results and references on the subject.

10.8. *Vaccination and mitigation measures*

Vaccination and exclusion by temporary confinement or physical barriers (masks, antiviral protection, or anti-transmission intermediates) are the public health measures intended to mitigate or stop an epidemic. The modeling of their gradual introduction and their effects on the spread of the epidemic makes it possible to understand their effectiveness or, on the contrary, their uselessness and, therefore, to adapt the coercive measures best, whether collective or individual [204–218].

10.9. *Chronological age*

The problem of age structure is crucial in epidemic modeling for three reasons:

- (i) The immune system efficacy depends on age. Therefore, its adaptive component is less and less able to resist a new pathogenic agent or react to a vaccine;
- (ii) Age groups communicate differently with each other, with the most mobile (working age group) having the greatest chance of transmission and the most dependent (elderlies) on the care by younger caregivers having the greatest chance of being infected;
- (iii) The prevalence of chronic diseases favoring infections is very unevenly distributed, the age groups at both ends of life being the most susceptible: the young due to the immaturity of the immune system and school promiscuity, and the elderly due to the existence of chronic comorbidities (diabetes, respiratory pathologies, cardiovascular diseases, and immune depression).

These disparities make it necessary to take age into account (through at least three major classes, young people under 20, adults from 20 to 65, and seniors over 65), preventive measures (education, vaccination, isolation) being taken according to this age stratification, crossed with the risk factors linked to the occurrence of chronic pathologies.

Few papers combined epidemic model with age-structure and age structured data [108,219–228]. The problem of understanding the relationships between data and models is far from well understood. In Section 9, based on [61], we proposed an approach to understanding how to connect the model and the data during the exponential phase. But such a problem needs further investigation.

10.10. Basic reproduction number

The basic reproduction number R_0 is an essential parameter for predicting the occurrence of an epidemic wave. It can vary over time and depends on two main factors:

- (i) In the infectious subject, the successive establishment of natural defense mechanisms (innate and adaptive) explains the variations in daily R_0 during his period of contagiousness;
- (ii) In subjects who are not yet infected, their susceptibility is also dependent on their immune status, but also on the collective public health measures taken at the population level.

Methods for estimating daily R_0 are therefore fundamental to understanding the temporal and spatial evolution of a pandemic [229–234].

10.11. Prediction of COVID-19 evolution

The difficulty of predicting the evolution of a pandemic is due to the adaptive capacities of the infectious agent and the infected and transmitting host. On the one hand, the genetic mutations of the infectious agent and its contagious power and pathogenic dangerousness develop a highly infectious and low pathogenic variant, often signaling the natural end of a pandemic. On the other hand, the permanent adaptation strategy of individual and collective host defense measures makes it possible to anticipate the effects of changes in the agent's infectious strategy. In both cases, modeling the dynamics of mutation and prevention is essential to predict and act in near real-time on the evolution of a pandemic [12,235–242].

Appendix

Appendix A When the output is a single exponential function

Let $X \in \mathbb{R}^n$. We recall that

- $X \geq 0$ if for each $i \in \{1, \dots, n\}$ such that $X_i \geq 0$;
- $X > 0$ if $X \geq 0$ and there exists $i \in \{1, \dots, n\}$ such that $X_i > 0$;
- $X \gg 0$ if $X_i > 0$ for each $i \in \{1, \dots, n\}$.

Let $A = (a_{ij}) \in M_n(\mathbb{R})$ a $n \times n$ matrix with non-negative off-diagonal elements, and assume that $A + \delta I$ is non-negative irreducible whenever $\delta > 0$ is large enough. The projector associated to the Perron-Frobenius dominant eigenvalue is defined by

$$\Pi x = \frac{\langle V_L(A), x \rangle V_R(A)}{\langle V_L(A), V_R(A) \rangle}, \forall x \in \mathbb{R}^n, \quad (\text{A1})$$

where $V_R(A) \gg 0$ (respectively $V_L(A) \gg 0$) is a right eigenvector (resp. left eigenvector) of A associated with the dominant eigenvalue

$$s(A) = \max\{\operatorname{Re} \lambda : \lambda \in \sigma(A)\},$$

where $\sigma(A)$ is the spectrum of A (i.e. the set of all eigenvalues of A). Then we have

$$A\Pi = \Pi A = s(A)\Pi.$$

Recall that the euclidean inner product is defined by

$$\langle X, Y \rangle = \sum_{i=1}^n X_i Y_i.$$

The network associated with a non-negative matrix A corresponds to all the oriented paths from the node i to the node j whenever $a_{ij} > 0$.

A non-negative matrix A is *irreducible* if the network associated with A is strongly connected. That is, if we can join any two nodes i and j by using a succession of oriented paths.

To understand irreducible matrices in epidemics, one may consider the contact matrix in epidemic models. Then, the contact matrix is irreducible if any infected sub-group has a non-zero probability of infecting any other group (by transmitting the pathogen to intermediate sub-groups if needed).

Theorem A1. *Let $A = (a_{ij}) \in M_n(\mathbb{R})$, and assume that the off-diagonal elements of A are non-negative, and $A + \delta I$ is non-negative irreducible whenever $\delta > 0$ is large enough. We assume that there exists a vector $X_0 > 0$ such that*

$$X'(t) = AX(t), \forall t \in [0, \tau], \text{ with } X(0) = X_0, \quad (\text{A2})$$

and there exists a vector $Y > 0$ satisfying

$$\sum_{i=1}^n Y_i X_i(t) = \chi_1 e^{\chi_2 t}, \forall t \in [0, \tau], \quad (\text{A3})$$

with $\chi_1 > 0$, $\chi_2 > 0$, and $\tau > 0$.

Then we have

$$\chi_2 = s(A), \text{ and } \chi_1 = \langle Y, \Pi X_0 \rangle.$$

That is,

$$\sum_{i=1}^n Y_i X_i(t) = \langle Y, \Pi X_0 \rangle e^{s(A)t}, \forall t \geq 0.$$

In other words, we can not distinguish the growth induced by $\langle Y, X_0 \rangle$ and $\langle Y, \Pi X_0 \rangle$. Therefore we can replace X_0 with ΠX_0 , and the output $\langle Y, X(t) \rangle$ will be the same. 852
853

Proof. The equation (A3) is equivalent to

$$\langle Y, e^{At} X_0 \rangle = \chi_1 e^{\chi_2 t}, \forall t \in [0, \tau],$$

For each $\delta > 0$ large enough such that $A + \delta I$ is non-negative and primitive, we have

$$\langle Y, e^{(A+\delta I)t} X_0 \rangle = \chi_1 e^{(\chi_2 + \delta)t}, \forall t \in [0, \tau],$$

so by computing the derivatives on both sides of the above equation and taking $t = 0$, we obtain

$$\langle Y, (A + \delta I)^m X_0 \rangle = \chi_1 (\chi_2 + \delta)^m, \forall m \in \mathbb{N}.$$

But we have $r(A + \delta I) = s(A) + \delta$, and

$$\langle Y, \frac{(A + \delta I)^m}{r(A + \delta I)^m} X_0 \rangle = \chi_1 \frac{(\chi_2 + \delta)^m}{(s(A) + \delta)^m}, \forall m \in \mathbb{N},$$

and since the right-hand side of the above equality converges to $\langle Y, \Pi X_0 \rangle > 0$ (where $\Pi \gg 0$ is the projector defined in (41)), we deduce that

$$\lim_{m \rightarrow \infty} \frac{(\chi_2 + \delta)^m}{(s(A) + \delta)^m} = \frac{\langle Y, \Pi X_0 \rangle}{\chi_1} > 0,$$

and the result follows. \square 854

References 855

1. Oran, D.P.; Topol, E.J. Prevalence of asymptomatic SARS-CoV-2 infection: a narrative review. *Annals of internal medicine* **2020**, *173*, 362–367. 856
857
2. Rothe, C.; Schunk, M.; Sothmann, P.; Bretzel, G.; Froeschl, G.; Wallrauch, C.; Zimmer, T.; Thiel, V.; Janke, C.; Guggemos, W.; et al. Transmission of 2019-nCoV infection from an asymptomatic contact in Germany. *New England journal of medicine* **2020**, *382*, 970–971. 858
859
860
3. Nishiura, H.; Linton, N.M.; Akhmetzhanov, A.R. Serial interval of novel coronavirus (COVID-19) infections. *International journal of infectious diseases* **2020**, *93*, 284–286. 861
862
4. Bylicki, O.; Paleiron, N.; Janvier, F. An outbreak of COVID-19 on an aircraft carrier. *N Engl J Med* **2021**, *384*, 976–7. 863
864
5. Griette, Q.; Magal, P. Clarifying predictions for COVID-19 from testing data: The example of New York State. *Infectious Disease Modelling* **2021**, *6*, 273–283. 865
866
6. Magal, P.; Webb, G. The parameter identification problem for SIR epidemic models: identifying unreported cases. *Journal of mathematical biology* **2018**, *77*, 1629–1648. 867
868
7. Ducrot, A.; Magal, P.; Nguyen, T.; Webb, G. Identifying the number of unreported cases in SIR epidemic models. *Mathematical medicine and biology: A journal of the IMA* **2020**, *37*, 243–261. 869
870
871
8. Demongeot, J.; Griette, Q.; Magal, P. SI epidemic model applied to COVID-19 data in mainland China. *Royal Society Open Science* **2020**, *7*, 201878. 872
873
9. Liu, Z.; Magal, P.; Seydi, O.; Webb, G. Understanding unreported cases in the COVID-19 epidemic outbreak in Wuhan, China, and the importance of major public health interventions. *Biology* **2020**, *9*, 50. 874
875
876
10. Liu, Z.; Magal, P.; Seydi, O.; Webb, G. A COVID-19 epidemic model with latency period. *Infectious Disease Modelling* **2020**, *5*, 323–337. 877
878
11. Demongeot, J.; Magal, P. Spectral method in epidemic time series: Application to COVID-19 pandemic. *Biology* **2022**, *11*, 1825. 879
880

12. Roda, W.C.; Varughese, M.B.; Han, D.; Li, M.Y. Why is it difficult to accurately predict the COVID-19 epidemic? *Infectious disease modelling* **2020**, *5*, 271–281. 881
13. Smith, H.L. *Monotone dynamical systems: an introduction to the theory of competitive and cooperative systems: an introduction to the theory of competitive and cooperative systems*; Number 41, American Mathematical Soc., 1995. 882
14. Ducrot, A.; Griette, Q.; Liu, Z.; Magal, P. *Differential Equations and Population Dynamics I, Introductory approaches*; Springer, 2022. 883
15. Magal, P.; Ruan, S. Susceptible-infectious-recovered models revisited: From the individual level to the population level. *Mathematical biosciences* **2014**, *250*, 26–40. 884
16. Qiu, Y.; Chen, X.; Shi, W. Impacts of social and economic factors on the transmission of coronavirus disease 2019 (COVID-19) in China. *Journal of population economics* **2020**, *33*, 1127–1172. 885
17. Chowell, G.; Hengartner, N.W.; Castillo-Chavez, C.; Fenimore, P.W.; Hyman, J.M. The basic reproductive number of Ebola and the effects of public health measures: the cases of Congo and Uganda. *Journal of theoretical biology* **2004**, *229*, 119–126. 886
18. Augeraud-Véron, E. Lifting the COVID-19 lockdown: different scenarios for France. *Mathematical Modelling of Natural Phenomena* **2020**, *15*, 40. 887
19. Liu, Z.; Magal, P.; Seydi, O.; Webb, G. Predicting the cumulative number of cases for the COVID-19 epidemic in China from early data. *Mathematical Biosciences and Engineering* **2020**, *17*, 3040–3051. 888
20. Eikenberry, S.E.; Mancuso, M.; Iboi, E.; Phan, T.; Eikenberry, K.; Kuang, Y.; Kostelich, E.; Gumel, A.B. To mask or not to mask: Modeling the potential for face mask use by the general public to curtail the COVID-19 pandemic. *Infectious disease modelling* **2020**, *5*, 293–308. 889
21. Rocklöv, J.; Sjödin, H. High population densities catalyse the spread of COVID-19. *Journal of travel medicine* **2020**, *27*, taaa038. 890
22. Seligmann, H.; Vuillerme, N.; Demongeot, J. Summer COVID-19 third wave: faster high altitude spread suggests high UV adaptation. *MedRxiv* **2020**, pp. 2020–08. 891
23. Demongeot, J.; Flet-Berliac, Y.; Seligmann, H. Temperature decreases spread parameters of the new Covid-19 case dynamics. *Biology* **2020**, *9*, 94. 892
24. Wang, J.; Tang, K.; Feng, K.; Lv, W.; et al. High temperature and high humidity reduce the transmission of COVID-19. *Available at SSRN* **2020**, *3551767*, 2020b. 893
25. Guillon, P.; Clément, M.; Sébille, V.; Rivain, J.G.; Chou, C.F.; Ruvoën-Clouet, N.; Le Pendu, J. Inhibition of the interaction between the SARS-CoV spike protein and its cellular receptor by anti-histo-blood group antibodies. *Glycobiology* **2008**, *18*, 1085–1093. 894
26. Zeberg, H.; Pääbo, S. The major genetic risk factor for severe COVID-19 is inherited from Neanderthals. *Nature* **2020**, *587*, 610–612. 895
27. Zhou, F.; Yu, T.; Du, R.; Fan, G.; Liu, Y.; Liu, Z.; Xiang, J.; Wang, Y.; Song, B.; Gu, X.; et al. Clinical course and risk factors for mortality of adult inpatients with COVID-19 in Wuhan, China: a retrospective cohort study. *The lancet* **2020**, *395*, 1054–1062. 896
28. Hu, Z.; Song, C.; Xu, C.; Jin, G.; Chen, Y.; Xu, X.; Ma, H.; Chen, W.; Lin, Y.; Zheng, Y.; et al. Clinical characteristics of 24 asymptomatic infections with COVID-19 screened among close contacts in Nanjing, China. *Science China Life Sciences* **2020**, *63*, 706–711. 897
29. Ma, S.; Zhang, J.; Zeng, M.; Yun, Q.; Guo, W.; Zheng, Y.; Zhao, S.; Wang, M.H.; Yang, Z. Epidemiological parameters of coronavirus disease 2019: a pooled analysis of publicly reported individual data of 1155 cases from seven countries. *Medrxiv* **2020**, pp. 2020–03. 898
30. Li, R.; Pei, S.; Chen, B.; Song, Y.; Zhang, T.; Yang, W.; Shaman, J. Substantial undocumented infection facilitates the rapid dissemination of novel coronavirus (SARS-CoV-2). *Science* **2020**, *368*, 489–493. 899
31. Byrne, A.W.; McEvoy, D.; Collins, A.B.; Hunt, K.; Casey, M.; Barber, A.; Butler, F.; Griffin, J.; Lane, E.A.; McAloon, C.; et al. Inferred duration of infectious period of SARS-CoV-2: rapid scoping review and analysis of available evidence for asymptomatic and symptomatic COVID-19 cases. *BMJ open* **2020**, *10*, e039856. 900
32. WHO. Report of the WHO-China Joint Mission on Coronavirus Disease 2019 COVID-19. <https://www.who.int/docs/default-source/coronaviruse/who-china-joint-mission-on-covid-19-final-report.pdf>. 901
33. Yang, Z.; Zeng, Z.; Wang, K.; Wong, S.S.; Liang, W.; Zanin, M.; Liu, P.; Cao, X.; Gao, Z.; Mai, Z.; et al. Modified SEIR and AI prediction of the epidemics trend of COVID-19 in China under public health interventions. *Journal of thoracic disease* **2020**, *12*, 165. 902

34. London, W.P.; Yorke, J.A. Recurrent outbreaks of measles, chickenpox and mumps: I. Seasonal variation in contact rates. *American journal of epidemiology* **1973**, *98*, 453–468. 939
35. Yorke, J.A.; London, W.P. Recurrent outbreaks of measles, chickenpox and mumps: II. Systematic differences in contact rates and stochastic effects. *American journal of epidemiology* **1973**, *98*, 469–482. 940
36. Wang, W.; Ruan, S. Simulating the SARS outbreak in Beijing with limited data. *Journal of theoretical biology* **2004**, *227*, 369–379. 941
37. Smirnova, A.; deCamp, L.; Chowell, G. Forecasting epidemics through nonparametric estimation of time-dependent transmission rates using the SEIR model. *Bulletin of mathematical biology* **2019**, *81*, 4343–4365. 942
38. Haderler, K. Parameter identification in epidemic models. *Mathematical biosciences* **2011**, *229*, 185–189. 943
39. Bernoulli, D. Essai d’une nouvelle analyse de la mortalité causée par la petite vérole et des avantages de l’inoculation pour la prévenir. *Mémoire Académie Royale des Sciences de Mathématique et de Physiques, Paris* **1766**. 944
40. Dietz, K.; Heesterbeek, J. Daniel Bernoulli’s epidemiological model revisited. *Mathematical biosciences* **2002**, *180*, 1–21. 945
41. Bernoulli, D.; Blower, S. An attempt at a new analysis of the mortality caused by smallpox and of the advantages of inoculation to prevent it. *Reviews in medical virology* **2004**, *14*, 275. 946
42. Bernoulli, D.; Chapelle, D. Essai d’une nouvelle analyse de la mortalité causée par la petite vérole, et des avantages de l’inoculation pour la prévenir. *HAL Id: hal-04100467* **2023**. 947
43. Verhulst, P.F. Notice sur la loi que la population suit dans son accroissement. *Correspondence mathématique et physique* **1838**, *10*, 113–129. 948
44. Hsieh, Y.H. Richards model: a simple procedure for real-time prediction of outbreak severity. In *Modeling and dynamics of infectious diseases*; World Scientific, 2009; pp. 216–236. 949
45. Wang, X.S.; Wu, J.; Yang, Y. Richards model revisited: Validation by and application to infection dynamics. *Journal of theoretical biology* **2012**, *313*, 12–19. 950
46. Zhou, G.; Yan, G. Severe acute respiratory syndrome epidemic in Asia. *Emerging infectious diseases* **2003**, *9*, 1608–1610. 951
47. Tsoularis, A.; Wallace, J. Analysis of logistic growth models. *Mathematical biosciences* **2002**, *179*, 21–55. 952
48. Bürger, R.; Chowell, G.; Lara-Díaz, L.Y. Comparative analysis of phenomenological growth models applied to epidemic outbreaks. *Mathematical Biosciences and Engineering* **2019**, *16*, 4250–4273. 953
49. Pelinovsky, E.; Kokoulina, M.; Epifanova, A.; Kurkin, A.; Kurkina, O.; Tang, M.; Macau, E.; Kirillin, M. Gompertz model in COVID-19 spreading simulation. *Chaos, Solitons & Fractals* **2022**, *154*, 111699. 954
50. Pelinovsky, E.; Kurkin, A.; Kurkina, O.; Kokoulina, M.; Epifanova, A. Logistic equation and COVID-19. *Chaos, Solitons & Fractals* **2020**, *140*, 110241. 955
51. Griette, Q.; Demongeot, J.; Magal, P. A robust phenomenological approach to investigate COVID-19 data for France. *Mathematics in Applied Sciences and Engineering* **2021**, *2*, 149–160. 956
52. Griette, Q.; Demongeot, J.; Magal, P. What can we learn from COVID-19 data by using epidemic models with unidentified infectious cases? *Mathematical Biosciences and Engineering* **2022**, *19*, 537–594. 957
53. Bakhta, A.; Boiveau, T.; Maday, Y.; Mula, O. Epidemiological forecasting with model reduction of compartmental models. application to the COVID-19 pandemic. *Biology* **2021**, *10*, 22. 958
54. Obadia, T.; Haneef, R.; Boëlle, P.Y. The R_0 package: a toolbox to estimate reproduction numbers for epidemic outbreaks. *BMC medical informatics and decision making* **2012**, *12*, 1–9. 959
55. Cori, A.; Ferguson, N.M.; Fraser, C.; Cauchemez, S. A new framework and software to estimate time-varying reproduction numbers during epidemics. *American journal of epidemiology* **2013**, *178*, 1505–1512. 960
56. Thompson, R.N.; Stockwin, J.E.; van Gaalen, R.D.; Polonsky, J.A.; Kamvar, Z.N.; Demarsh, P.A.; Dahlqwert, E.; Li, S.; Miguel, E.; Jombart, T.; et al. Improved inference of time-varying reproduction numbers during infectious disease outbreaks. *Epidemics* **2019**, *29*, 100356. 961
57. Demongeot, J.; Magal, P.; Oshnubi, K. Forecasting the changes between endemic and epidemic phases of a contagious disease, with the example of COVID-19. *Submitted*. 962

58. Arino, J.; Brauer, F.; van den Driessche, P.; Watmough, J.; Wu, J. Simple models for containment of a pandemic. *Journal of the Royal Society Interface* **2006**, *3*, 453–457. 998
59. Regan, D.; Wood, J.; Benevent, C.; Ali, H.; Smith, L.W.; Robertson, P.; Ferson, M.; Fairley, C.; Donovan, B.; Law, M. Estimating the critical immunity threshold for preventing hepatitis A outbreaks in men who have sex with men. *Epidemiology & Infection* **2016**, *144*, 1528–1537. 999
60. Liu, Z.; Magal, P.; Webb, G. Predicting the number of reported and unreported cases for the COVID-19 epidemics in China, South Korea, Italy, France, Germany and United Kingdom. *Journal of Theoretical Biology* **2021**, *509*, 110501. 1000
61. Griette, Q.; Magal, P.; Seydi, O. Unreported cases for age dependent COVID-19 outbreak in Japan. *Biology* **2020**, *9*, 132. 1001
62. Prem, K.; Cook, A.R.; Jit, M. Projecting social contact matrices in 152 countries using contact surveys and demographic data. *PLoS computational biology* **2017**, *13*, e1005697. 1002
63. WHO. COVID-19 Research Database. <https://search.bvsalud.org/global-literature-on-novel-coronavirus-2019-ncov/>. 1003
64. Ioannidis, J.P.; Salholz-Hillel, M.; Boyack, K.W.; Baas, J. The rapid, massive growth of COVID-19 authors in the scientific literature. *Royal Society open science* **2021**, *8*, 210389. 1004
65. Rodriguez-Morales, A.J.; Cardona-Ospina, J.A.; Gutiérrez-Ocampo, E.; Villamizar-Peña, R.; Holguin-Rivera, Y.; Escalera-Antezana, J.P.; Alvarado-Arnez, L.E.; Bonilla-Aldana, D.K.; Franco-Paredes, C.; Henao-Martinez, A.F.; et al. Clinical, laboratory and imaging features of COVID-19: A systematic review and meta-analysis. *Travel medicine and infectious disease* **2020**, *34*, 101623. 1005
66. IDO. Infectious Disease Outbreaks webinar. <https://www.math.u-bordeaux.fr/~pmagal100p/webinar2020.html>. 1006
67. Azevedo, F.M.; Morais, N.d.S.d.; Silva, D.L.F.; Candido, A.C.; Morais, D.d.C.; Priore, S.E.; Franceschini, S.d.C.C. Food insecurity and its socioeconomic and health determinants in pregnant women and mothers of children under 2 years of age, during the COVID-19 pandemic: A systematic review and meta-analysis. *Frontiers in Public Health* **2023**, *11*, 1087955. 1007
68. Tille, F.; Van Ginneken, E.; Winkelmann, J.; Hernandez-Quevedo, C.; Falkenbach, M.; Sagan, A.; Karanikolos, M.; Cylus, J. Perspective: Lessons from COVID-19 of countries in the European region in light of findings from the health system response monitor. *Frontiers in public health* **2023**, *10*, 1058729. 1008
69. Lu, W.; Ren, H. Diseases spectrum in the field of spatiotemporal patterns mining of infectious diseases epidemics: A bibliometric and content analysis. *Frontiers in Public Health* **2023**, *10*, 1089418. 1009
70. Chen, X.; Zhang, C.; Ibrahim, S.; Tao, S.; Xia, X.; Li, Y.; Li, C.; Yue, F.; Wang, X.; Bao, S.; et al. The impact of facemask on patients with COPD: A systematic review and meta-analysis. *Frontiers in public health* **2022**, *10*, 1027521. 1010
71. Hu, Z.; Song, C.; Xu, C.; Jin, G.; Chen, Y.; Xu, X.; Ma, H.; Chen, W.; Lin, Y.; Zheng, Y.; et al. Clinical characteristics of 24 asymptomatic infections with COVID-19 screened among close contacts in Nanjing, China. *Science China Life Sciences* **2020**, *63*, 706–711. 1011
72. Arons, M.M.; Hatfield, K.M.; Reddy, S.C.; Kimball, A.; James, A.; Jacobs, J.R.; Taylor, J.; Spicer, K.; Bardossy, A.C.; Oakley, L.P.; et al. Presymptomatic SARS-CoV-2 infections and transmission in a skilled nursing facility. *New England journal of medicine* **2020**, *382*, 2081–2090. 1012
73. Pan, Y.; Yu, X.; Du, X.; Li, Q.; Li, X.; Qin, T.; Wang, M.; Jiang, M.; Li, J.; Li, W.; et al. Epidemiological and clinical characteristics of 26 asymptomatic severe acute respiratory syndrome coronavirus 2 carriers. *The Journal of infectious diseases* **2020**, *221*, 1940–1947. 1013
74. Böhmer, M.M.; Buchholz, U.; Corman, V.M.; Hoch, M.; Katz, K.; Marosevic, D.V.; Böhm, S.; Woudenberg, T.; Ackermann, N.; Konrad, R.; et al. Investigation of a COVID-19 outbreak in Germany resulting from a single travel-associated primary case: a case series. *The Lancet Infectious Diseases* **2020**, *20*, 920–928. 1014
75. Ciotti, M.; Ciccozzi, M.; Terrinoni, A.; Jiang, W.C.; Wang, C.B.; Bernardini, S. The COVID-19 pandemic. *Critical reviews in clinical laboratory sciences* **2020**, *57*, 365–388. 1015
76. Shi, Y.; Wang, G.; Cai, X.p.; Deng, J.w.; Zheng, L.; Zhu, H.h.; Zheng, M.; Yang, B.; Chen, Z. An overview of COVID-19. *Journal of Zhejiang University. Science. B* **2020**, *21*, 343. 1016
77. Nalbandian, A.; Sehgal, K.; Gupta, A.; Madhavan, M.V.; McGroder, C.; Stevens, J.S.; Cook, J.R.; Nordvig, A.S.; Shalev, D.; Sehwat, T.S.; et al. Post-acute COVID-19 syndrome. *Nature medicine* **2021**, *27*, 601–615. 1017

78. Wang, C.C.; Prather, K.A.; Sznitman, J.; Jimenez, J.L.; Lakdawala, S.S.; Tufekci, Z.; Marr, L.C. Airborne transmission of respiratory viruses. *Science* **2021**, *373*, eabd9149. 1056
79. Schippers, M.C.; Ioannidis, J.; Joffe, A.R. Aggressive measures, rising inequalities, and mass formation during the COVID-19 crisis: An overview and proposed way forward. *Frontiers in public health* **2022**, p. 2715. 1058
80. Kolaski, K.; Logan, L.R.; Ioannidis, J.P. Improving systematic reviews: guidance on guidance and other options and challenges. *Journal of Clinical Epidemiology* **2023**. 1060
81. Hirt, J.; Janiaud, P.; Gloy, V.L.; Schandelmaier, S.; Pereira, T.V.; Contopoulos-Ioannidis, D.; Goodman, S.N.; Ioannidis, J.; Munkholm, K.; Hemkens, L.G. Robustness of reported postacute health outcomes in children with SARS-CoV-2 infection: a systematic review. *Archives of Disease in Childhood* **2023**, *108*, 498–505. 1062
82. Zhao, Q. Small data, big time—a retrospect of the first weeks of COVID-19. *Journal of the Royal Statistical Society Series A: Statistics in Society* **2022**, *185*, 1793–1814. 1064
83. Jones, T.C.; Biele, G.; Mühlemann, B.; Veith, T.; Schneider, J.; Beheim-Schwarzbach, J.; Bleicker, T.; Tesch, J.; Schmidt, M.L.; Sander, L.E.; et al. Estimating infectiousness throughout SARS-CoV-2 infection course. *Science* **2021**, *373*, eabi5273. 1066
84. He, X.; Lau, E.H.; Wu, P.; Deng, X.; Wang, J.; Hao, X.; Lau, Y.C.; Wong, J.Y.; Guan, Y.; Tan, X.; et al. Temporal dynamics in viral shedding and transmissibility of COVID-19. *Nature medicine* **2020**, *26*, 672–675. 1068
85. Linton, N.M.; Kobayashi, T.; Yang, Y.; Hayashi, K.; Akhmetzhanov, A.R.; Jung, S.m.; Yuan, B.; Kinoshita, R.; Nishiura, H. Incubation period and other epidemiological characteristics of 2019 novel coronavirus infections with right truncation: a statistical analysis of publicly available case data. *Journal of clinical medicine* **2020**, *9*, 538. 1070
86. Wu, Y.; Kang, L.; Guo, Z.; Liu, J.; Liu, M.; Liang, W. Incubation period of COVID-19 caused by unique SARS-CoV-2 strains: a systematic review and meta-analysis. *JAMA network open* **2022**, *5*, e2228008–e2228008. 1072
87. Quesada, J.; López-Pineda, A.; Gil-Guillén, V.; Arriero-Marín, J.; Gutiérrez, F.; Carratala-Munuera, C. Incubation period of COVID-19: A systematic review and meta-analysis. *Revista Clínica Española (English Edition)* **2021**, *221*, 109–117. 1074
88. Rai, B.; Shukla, A.; Dwivedi, L.K. Incubation period for COVID-19: a systematic review and meta-analysis. *Journal of Public Health* **2021**, pp. 1–8. 1076
89. Zuo, Y.Y.; Uspal, W.E.; Wei, T. Airborne transmission of COVID-19: aerosol dispersion, lung deposition, and virus-receptor interactions. *ACS nano* **2020**, *14*, 16502–16524. 1078
90. Demongeot, J.; Griette, Q.; Maday, Y.; Magal, P. A Kermack–McKendrick model with age of infection starting from a single or multiple cohorts of infected patients. *Proceedings of the Royal Society A* **2023**, *479*, 20220381. 1080
91. Alvarez, L.; Colom, M.; Morel, J.D.; Morel, J.M. Computing the daily reproduction number of COVID-19 by inverting the renewal equation using a variational technique. *Proceedings of the National Academy of Sciences* **2021**, *118*, e2105112118. 1082
92. Rowe, F.; Ngwenyama, O.; Richet, J.L. Contact-tracing apps and alienation in the age of COVID-19. *European Journal of Information Systems* **2020**, *29*, 545–562. 1084
93. Kapa, S.; Halamka, J.; Raskar, R. Contact tracing to manage COVID-19 spread—balancing personal privacy and public health. In *Proceedings of the Mayo Clinic Proceedings*. Elsevier, 2020, Vol. 95, pp. 1320–1322. 1086
94. Kretzschmar, M.E.; Rozhnova, G.; Bootsma, M.C.; van Boven, M.; van de Wijkert, J.H.; Bonten, M.J. Impact of delays on effectiveness of contact tracing strategies for COVID-19: a modelling study. *The Lancet Public Health* **2020**, *5*, e452–e459. 1088
95. Browne, C.J.; Gulbudak, H.; Macdonald, J.C. Differential impacts of contact tracing and lockdowns on outbreak size in COVID-19 model applied to China. *Journal of Theoretical Biology* **2022**, *532*, 110919. 1090
96. Hart, W.S.; Maini, P.K.; Thompson, R.N. High infectiousness immediately before COVID-19 symptom onset highlights the importance of continued contact tracing. *Elife* **2021**, *10*, e65534. 1092
97. Giovanetti, M.; Cella, E.; Benedetti, F.; Rife Magalis, B.; Fonseca, V.; Fabris, S.; Campisi, G.; Ciccozzi, A.; Angeletti, S.; Borsetti, A.; et al. SARS-CoV-2 shifting transmission dynamics and hidden reservoirs potentially limit efficacy of public health interventions in Italy. *Communications biology* **2021**, *4*, 489. 1094
98. Zanella, M.; Bardelli, C.; Azzi, M.; Deandrea, S.; Perotti, P.; Silva, S.; Cadum, E.; Figini, S.; Toscani, G. Social contacts, epidemic spreading and health system. *Mathematical modeling* 1096

- and applications to COVID-19 infection. *Machine Learning and Statistical models in real world applications* **2021**, p. 83. 1114
99. Bode, M.; Craven, M.; Leopoldseeder, M.; Rutten, P.; Wilson, M. Contact tracing for COVID-19: New considerations for its practical application. *McKinsey & Company* **2020**, p. 8. 1115
100. Martinez-Martin, N.; Wieten, S.; Magnus, D.; Cho, M.K. Digital contact tracing, privacy, and public health. *Hastings Center Report* **2020**, *50*, 43–46. 1116
101. Blasimme, A.; Ferretti, A.; Vayena, E. Digital contact tracing against COVID-19 in Europe: current features and ongoing developments. *Frontiers in Digital Health* **2021**, *3*, 660823. 1117
102. Jian, S.W.; Cheng, H.Y.; Huang, X.T.; Liu, D.P. Contact tracing with digital assistance in Taiwan’s COVID-19 outbreak response. *International Journal of Infectious Diseases* **2020**, *101*, 348–352. 1118
103. Thayyil, J.; Kuniyil, V.; Cherumanalil, J.M. COVID-19: digital contact tracing technologies and ethical challenges. *Int J Community Med Public Health* **2020**, *7*, 2854. 1119
104. Cho, H.; Ippolito, D.; Yu, Y.W. Contact tracing mobile apps for COVID-19: Privacy considerations and related trade-offs. *arXiv preprint arXiv:2003.11511* **2020**. 1120
105. Peccoud, J.; Jacob, C. Theoretical uncertainty of measurements using quantitative polymerase chain reaction. *Biophysical journal* **1996**, *71*, 101–108. 1121
106. Peccoud, J.; Jacob, C. Statistical estimations of PCR amplification rates. In *Gene Quantification*; 1998; pp. 111–128. 1122
107. Hellewell, J.; Russell, T.W.; Beale, R.; Kelly, G.; Houlihan, C.; Nastouli, E.; Kucharski, A.J. Estimating the effectiveness of routine asymptomatic PCR testing at different frequencies for the detection of SARS-CoV-2 infections. *BMC medicine* **2021**, *19*, 1–10. 1123
108. Kretzschmar, M.E.; Ashby, B.; Fearon, E.; Overton, C.E.; Panovska-Griffiths, J.; Pellis, L.; Quaife, M.; Rozhnova, G.; Scarabel, F.; Stage, H.B.; et al. Challenges for modelling interventions for future pandemics. *Epidemics* **2022**, *38*, 100546. 1124
109. Kucirka, L.M.; Lauer, S.A.; Laeyendecker, O.; Boon, D.; Lessler, J. Variation in false-negative rate of reverse transcriptase polymerase chain reaction–based SARS-CoV-2 tests by time since exposure. *Annals of internal medicine* **2020**, *173*, 262–267. 1125
110. Böger, B.; Fachi, M.M.; Vilhena, R.O.; Cobre, A.F.; Tonin, F.S.; Pontarolo, R. Systematic review with meta-analysis of the accuracy of diagnostic tests for COVID-19. *American journal of infection control* **2021**, *49*, 21–29. 1126
111. Salvatore, P.P.; Lee, C.C.; Sleweon, S.; McCormick, D.W.; Nicolae, L.; Knipe, K.; Dixon, T.; Banta, R.; Ogle, I.; Young, C.; et al. Transmission potential of vaccinated and unvaccinated persons infected with the SARS-CoV-2 Delta variant in a federal prison, July–August 2021. *Vaccine* **2023**, *41*, 1808–1818. 1127
112. Arevalo-Rodriguez, I.; Buitrago-Garcia, D.; Simancas-Racines, D.; Zambrano-Achig, P.; Del Campo, R.; Ciapponi, A.; Sued, O.; Martinez-Garcia, L.; Rutjes, A.W.; Low, N.; et al. False-negative results of initial RT-PCR assays for COVID-19: a systematic review. *PloS one* **2020**, *15*, e0242958. 1128
113. Pu, R.; Liu, S.; Ren, X.; Shi, D.; Ba, Y.; Huo, Y.; Zhang, W.; Ma, L.; Liu, Y.; Yang, Y.; et al. The screening value of RT-LAMP and RT-PCR in the diagnosis of COVID-19: systematic review and meta-analysis. *Journal of virological methods* **2022**, *300*, 114392. 1129
114. Bugalia, S.; Tripathi, J.P. Assessing potential insights of an imperfect testing strategy: Parameter estimation and practical identifiability using early COVID-19 data in India. *Communications in Nonlinear Science and Numerical Simulation* **2023**, *123*, 107280. 1130
115. Aronna, M.S.; Guglielmi, R.; Moschen, L.M. Estimate of the rate of unreported COVID-19 cases during the first outbreak in Rio de Janeiro. *Infectious Disease Modelling* **2022**, *7*, 317–332. 1131
116. Chow, C.C.; Chang, J.C.; Gerkin, R.C.; Vattikuti, S. Global prediction of unreported SARS-CoV2 infection from observed COVID-19 cases. *MedRxiv* **2020**. 1132
117. Hortaçsu, A.; Liu, J.; Schwieg, T. Estimating the fraction of unreported infections in epidemics with a known epicenter: An application to COVID-19. *Journal of Econometrics* **2021**, *220*, 106–129. 1133
118. Reis, R.F.; de Melo Quintela, B.; de Oliveira Campos, J.; Gomes, J.M.; Rocha, B.M.; Lobosco, M.; Dos Santos, R.W. Characterization of the COVID-19 pandemic and the impact of uncertainties, mitigation strategies, and underreporting of cases in South Korea, Italy, and Brazil. *Chaos, Solitons & Fractals* **2020**, *136*, 109888. 1134

119. Zhao, S.; Musa, S.S.; Lin, Q.; Ran, J.; Yang, G.; Wang, W.; Lou, Y.; Yang, L.; Gao, D.; He, D.; et al. Estimating the unreported number of novel coronavirus (2019-nCoV) cases in China in the first half of January 2020: a data-driven modelling analysis of the early outbreak. *Journal of clinical medicine* **2020**, *9*, 388. 1172-1175
120. Huo, X.; Chen, J.; Ruan, S. Estimating asymptomatic, undetected and total cases for the COVID-19 outbreak in Wuhan: a mathematical modeling study. *BMC infectious diseases* **2021**, *21*, 476. 1176-1178
121. Oladipo, S.; Sun, Y.; Amole, A. Performance evaluation of the impact of clustering methods and parameters on adaptive neuro-fuzzy inference system models for electricity consumption prediction during COVID-19. *Energies* **2022**, *15*, 7863. 1179-1181
122. Ito, H.; Chakraborty, B. Social media mining with dynamic clustering: a case study by COVID-19 tweets. In Proceedings of the 2020 11th International Conference on Awareness Science and Technology (iCAST). IEEE, 2020, pp. 1–6. 1182-1184
123. Andrade, L.; Gomes, D.; Lima, S.; Duque, A.; Melo, M.; Góes, M.; Ribeiro, C.; Peixoto, M.; Souza, C.; Santos, A. COVID-19 mortality in an area of northeast Brazil: epidemiological characteristics and prospective spatiotemporal modelling. *Epidemiology & Infection* **2020**, *148*, e288. 1185-1188
124. Nazia, N.; Butt, Z.A.; Bedard, M.L.; Tang, W.C.; Sehar, H.; Law, J. Methods used in the spatial and spatiotemporal analysis of COVID-19 epidemiology: a systematic review. *International Journal of Environmental Research and Public Health* **2022**, *19*, 8267. 1189-1191
125. Harris, J.E. Geospatial analysis of a COVID-19 outbreak at the University of Wisconsin–Madison: potential role of a cluster of local bars. *Epidemiology & Infection* **2022**, *150*, e76. 1192-1193
126. Gomes, D.S.; Andrade, L.A.; Ribeiro, C.J.N.; Peixoto, M.; Lima, S.; Duque, A.; Cirilo, T.M.; Góes, M.; Lima, A.; Santos, M.; et al. Risk clusters of COVID-19 transmission in northeastern Brazil: prospective space–time modelling. *Epidemiology & Infection* **2020**, *148*, e188. 1194-1196
127. Adam, D.C.; Wu, P.; Wong, J.Y.; Lau, E.H.; Tsang, T.K.; Cauchemez, S.; Leung, G.M.; Cowling, B.J. Clustering and superspreading potential of SARS-CoV-2 infections in Hong Kong. *Nature Medicine* **2020**, *26*, 1714–1719. 1197-1199
128. Chan, J.F.W.; Yuan, S.; Kok, K.H.; To, K.K.W.; Chu, H.; Yang, J.; Xing, F.; Liu, J.; Yip, C.C.Y.; Poon, R.W.S.; et al. A familial cluster of pneumonia associated with the 2019 novel coronavirus indicating person-to-person transmission: a study of a family cluster. *The lancet* **2020**, *395*, 514–523. 1200-1203
129. Ma, J. Estimating epidemic exponential growth rate and basic reproduction number. *Infectious Disease Modelling* **2020**, *5*, 129–141. 1204-1205
130. Tat Dat, T.; Frédéric, P.; Hang, N.T.; Jules, M.; Duc Thang, N.; Piffault, C.; Willy, R.; Susely, F.; Lê, H.V.; Tuschmann, W.; et al. Epidemic dynamics via wavelet theory and machine learning with applications to COVID-19. *Biology* **2020**, *9*, 477. 1206-1208
131. Miyama, T.; Jung, S.m.; Hayashi, K.; Anzai, A.; Kinoshita, R.; Kobayashi, T.; Linton, N.M.; Suzuki, A.; Yang, Y.; Yuan, B.; et al. Phenomenological and mechanistic models for predicting early transmission data of COVID-19. *Math. Biosci. Eng* **2022**, *19*, 2043–2055. 1209-1211
132. Attanayake, A.; Perera, S.; Jayasinghe, S. Phenomenological Modelling of COVID-19 epidemics in Sri Lanka, Italy and Hebei Province of China. *MedRxiv* **2020**, pp. 2020–05. 1212-1213
133. Zuhairroh, F.; Rosadi, D. Data-driven analysis and prediction of COVID-19 infection in Southeast Asia by using a phenomenological model. *Pakistan Journal of Statistics and Operation Research* **2022**, *18*, 59–69. 1214-1216
134. Calatayud, J.; Jornet, M.; Mateu, J. A phenomenological model for COVID-19 data taking into account neighboring-provinces effect and random noise. *Statistica Neerlandica* **2023**, *77*, 146–155. 1217-1219
135. Smith, B.A.; Bancej, C.; Fazil, A.; Mullah, M.; Yan, P.; Zhang, S. The performance of phenomenological models in providing near-term Canadian case projections in the midst of the COVID-19 pandemic: March–April, 2020. *Epidemics* **2021**, *35*, 100457. 1220-1222
136. Richards, F.J. A flexible growth function for empirical use. *Journal of experimental Botany* **1959**, *10*, 290–301. 1223-1224
137. Sari, G.L.; Hilmi, I.L.; Nurdiana, A.; Azizah, A.N.; Kasasiah, A. Infectious waste management as the effects of COVID-19 pandemic in Indonesia. *Asian Journal of Social Science and Management Technology* **2021**, *3*, 62–75. 1225-1227
138. Elsaid, K.; Olabi, V.; Sayed, E.T.; Wilberforce, T.; Abdelkareem, M.A. Effects of COVID-19 on the environment: an overview on air, water, wastewater, and solid waste. *Journal of Environmental Management* **2021**, *292*, 112694. 1228-1230

139. Ai, Y.; Davis, A.; Jones, D.; Lemeshow, S.; Tu, H.; He, F.; Ru, P.; Pan, X.; Bohrerova, Z.; Lee, J. Wastewater SARS-CoV-2 monitoring as a community-level COVID-19 trend tracker and variants in Ohio, United States. *Science of The Total Environment* **2021**, *801*, 149757. 1231-1233
140. Bertrand, I.; Challant, J.; Jeulin, H.; Hartard, C.; Mathieu, L.; Lopez, S.; Obépine, S.I.G.; Schvoerer, E.; Courtois, S.; Gantzer, C. Epidemiological surveillance of SARS-CoV-2 by genome quantification in wastewater applied to a city in the northeast of France: Comparison of ultrafiltration-and protein precipitation-based methods. *International Journal of Hygiene and Environmental Health* **2021**, *233*, 113692. 1234-1238
141. Gragnani, L.; Monti, M.; Santini, S.A.; Marri, S.; Madia, F.; Lorini, S.; Petraccia, L.; Stasi, C.; Basile, U.; Luti, V.; et al. SARS-CoV-2 was already circulating in Italy, in early December 2019. *European Review for Medical & Pharmacological Sciences* **2021**, *25*. 1239-1240
142. Wurtzer, S.; Waldman, P.; Levert, M.; Cluzel, N.; Almayrac, J.; Charpentier, C.; Masnada, S.; Gillon-Ritz, M.; Mouchel, J.; Maday, Y.; et al. SARS-CoV-2 genome quantification in wastewaters at regional and city scale allows precise monitoring of the whole outbreaks dynamics and variants spreading in the population. *Science of The Total Environment* **2022**, *810*, 152213. 1241-1246
143. Wurtzer, S.; Waldman, P.; Ferrier-Rembert, A.; Frenois-Veyrat, G.; Mouchel, J.M.; Boni, M.; Maday, Y.; Marechal, V.; Moulin, L.; et al. Several forms of SARS-CoV-2 RNA can be detected in wastewaters: implication for wastewater-based epidemiology and risk assessment. *Water Research* **2021**, *198*, 117183. 1247-1249
144. Wurtzer, S.; Marechal, V.; Mouchel, J.; Maday, Y.; Teyssou, R.; Richard, E.; Almayrac, J.; Moulin, e.L. Evaluation of lockdown effect on SARS-CoV-2 dynamics through viral genome quantification in waste water, Greater Paris, France, 5 March to 23 April 2020. *Eurosurveillance* **2020**, *25*, 2000776. 1250-1254
145. Zhou, L.; Rong, X.; Fan, M.; Yang, L.; Chu, H.; Xue, L.; Hu, G.; Liu, S.; Zeng, Z.; Chen, M.; et al. Modeling and evaluation of the joint prevention and control mechanism for curbing COVID-19 in Wuhan. *Bulletin of Mathematical Biology* **2022**, *84*, 28. 1255-1257
146. Xue, L.; Jing, S.; Miller, J.C.; Sun, W.; Li, H.; Estrada-Franco, J.G.; Hyman, J.M.; Zhu, H. A data-driven network model for the emerging COVID-19 epidemics in Wuhan, Toronto and Italy. *Mathematical biosciences* **2020**, *326*, 108391. 1258-1260
147. Forien, R.; Pang, G.; Pardoux, É. Estimating the state of the COVID-19 epidemic in France using a non-Markovian model. *medRxiv* **2020**, pp. 2020–06. 1261-1262
148. Bacallado, S.; Zhao, Q.; Ju, N. Generation interval for COVID-19 based on symptom onset data. *Eurosurveillance* **2020**, *25*, 2001381. 1263-1264
149. Demongeot, J.; Oshinubi, K.; Rachdi, M.; Hobbad, L.; Alahiane, M.; Iggui, S.; Gaudart, J.; Ouassou, I. The application of ARIMA model to analyze COVID-19 incidence pattern in several countries. *J. Math. Comput. Sci.* **2021**, *12*, Article-ID. 1265-1267
150. Soubeyrand, S.; Demongeot, J.; Roques, L. Towards unified and real-time analyses of outbreaks at country-level during pandemics. *One Health* **2020**, *11*, 100187. 1268-1269
151. Oshinubi, K.; Ibrahim, F.; Rachdi, M.; Demongeot, J. Functional data analysis: Application to daily observation of COVID-19 prevalence in France. *AIMS Mathematics* **2022**, *7*, 5347–5385. 1270-1271
152. Benhamou, W.; Lion, S.; Choquet, R.; Gandon, S. Phenotypic evolution of SARS-CoV-2: a statistical inference approach. *medRxiv* **2022**, pp. 2022–08. 1272-1273
153. Zhao, S.; Cao, P.; Gao, D.; Zhuang, Z.; Cai, Y.; Ran, J.; Chong, M.K.; Wang, K.; Lou, Y.; Wang, W.; et al. Serial interval in determining the estimation of reproduction number of the novel coronavirus disease (COVID-19) during the early outbreak. *Journal of travel medicine* **2020**, *27*, taaa033. 1274-1277
154. Gaudart, J.; Landier, J.; Huiart, L.; Legendre, E.; Lehot, L.; Bendiane, M.K.; Chiche, L.; Petitjean, A.; Mosnier, E.; Kirakoya-Samadoulougou, F.; et al. Factors associated with the spatial heterogeneity of the first wave of COVID-19 in France: a nationwide geo-epidemiological study. *The Lancet Public Health* **2021**, *6*, e222–e231. 1278-1281
155. Mizumoto, K.; Chowell, G. Transmission potential of the novel coronavirus (COVID-19) onboard the diamond Princess Cruises Ship, 2020. *Infectious disease modelling* **2020**, *5*, 264–270. 1282-1284
156. Tang, B.; Bragazzi, N.L.; Li, Q.; Tang, S.; Xiao, Y.; Wu, J. An updated estimation of the risk of transmission of the novel coronavirus (2019-nCov). *Infectious disease modelling* **2020**, *5*, 248–255. 1285-1286

157. Hart, W.S.; Abbott, S.; Endo, A.; Hellewell, J.; Miller, E.; Andrews, N.; Maini, P.K.; Funk, S.; Thompson, R.N. Inference of the SARS-CoV-2 generation time using UK household data. *Elife* **2022**, *11*, e70767. 1288–1290
158. Hart, W.S.; Miller, E.; Andrews, N.J.; Waight, P.; Maini, P.K.; Funk, S.; Thompson, R.N. Generation time of the alpha and delta SARS-CoV-2 variants: an epidemiological analysis. *The Lancet Infectious Diseases* **2022**, *22*, 603–610. 1291–1293
159. Morel, J.D.; Morel, J.M.; Alvarez, L. Learning from the past: a short term forecast method for the COVID-19 incidence curve. *PLoS Computational Biology* **2023**, *19*, e1010790. 1294–1295
160. Roosa, K.; Lee, Y.; Luo, R.; Kirpich, A.; Rothenberg, R.; Hyman, J.M.; Yan, P.; Chowell, G. Real-time forecasts of the COVID-19 epidemic in China from February 5th to February 24th, 2020. *Infectious disease modelling* **2020**, *5*, 256–263. 1296–1298
161. Renardy, M.; Eisenberg, M.; Kirschner, D. Predicting the second wave of COVID-19 in Washtenaw County, MI. *Journal of theoretical biology* **2020**, *507*, 110461. 1299–1300
162. Pullano, G.; Di Domenico, L.; Sabbatini, C.E.; Valdano, E.; Turbelin, C.; Debin, M.; Guerrisi, C.; Kengne-Kuetché, C.; Souty, C.; Hanslik, T.; et al. Underdetection of cases of COVID-19 in France threatens epidemic control. *Nature* **2021**, *590*, 134–139. 1301–1303
163. Modeling COVID-19 scenarios for the United States. *Nature medicine* **2021**, *27*, 94–105. 1304
164. Li, R.; Pei, S.; Chen, B.; Song, Y.; Zhang, T.; Yang, W.; Shaman, J. Substantial undocumented infection facilitates the rapid dissemination of novel coronavirus (SARS-CoV-2). *Science* **2020**, *368*, 489–493. 1305–1307
165. Giordano, G.; Blanchini, F.; Bruno, R.; Colaneri, P.; Di Filippo, A.; Di Matteo, A.; Colaneri, M. Modelling the COVID-19 epidemic and implementation of population-wide interventions in Italy. *Nature medicine* **2020**, *26*, 855–860. 1308–1309
166. Prague, M.; Wittkop, L.; Collin, A.; Dutartre, D.; Clairon, Q.; Moireau, P.; Thiebaut, R.; Hejblum, B.P. Multi-level modeling of early COVID-19 epidemic dynamics in French regions and estimation of the lockdown impact on infection rate. *MedRxiv* **2020**, pp. 2020–04. 1311–1312
167. Parolini, N.; Dede, L.; Antonietti, P.F.; Ardenghi, G.; Manzoni, A.; Miglio, E.; Pugliese, A.; Verani, M.; Quarteroni, A. SUIHTER: A new mathematical model for COVID-19. Application to the analysis of the second epidemic outbreak in Italy. *Proceedings of the Royal Society A* **2021**, *477*, 20210027. 1314–1317
168. Zhao, W.; Sun, Y.; Li, Y.; Guan, W. Prediction of COVID-19 Data Using Hybrid Modeling Approaches. *Frontiers in public health* **2022**, *10*, 923978. 1318–1319
169. Saiprasad, V.; Gopal, R.; Chandrasekar, V.; Lakshmanan, M. Analysis of COVID-19 in India using a vaccine epidemic model incorporating vaccine effectiveness and herd immunity. *The European Physical Journal Plus* **2022**, *137*, 1–11. 1320–1322
170. Thomas, D.M.; Sturdivant, R.; Dhurandhar, N.V.; Debroy, S.; Clark, N. A Primer on COVID-19 Mathematical Models. *Obesity (Silver Spring, Md.)* **2020**, *28*, 1375. 1323–1324
171. Alamo, T.; Reina, D.G.; Gata, P.M.; Preciado, V.M.; Giordano, G. Data-driven methods for present and future pandemics: Monitoring, modelling and managing. *Annual Reviews in Control* **2021**, *52*, 448–464. 1325–1327
172. Lin, Q.; Zhao, S.; Gao, D.; Lou, Y.; Yang, S.; Musa, S.S.; Wang, M.H.; Cai, Y.; Wang, W.; Yang, L.; et al. A conceptual model for the coronavirus disease 2019 (COVID-19) outbreak in Wuhan, China with individual reaction and governmental action. *International journal of infectious diseases* **2020**, *93*, 211–216. 1328–1330
173. Zanella, M.; Bardelli, C.; Dimarco, G.; Deandrea, S.; Perotti, P.; Azzi, M.; Figini, S.; Toscani, G. A data-driven epidemic model with social structure for understanding the COVID-19 infection on a heavily affected Italian Province. *Mathematical Models and Methods in Applied Sciences* **2021**, *31*, 2533–2570. 1331–1335
174. Meng, L.; Zhu, W. Generalized SEIR epidemic model for COVID-19 in a multipatch environment. *Discrete Dynamics in Nature and Society* **2021**, *2021*, 1–12. 1336–1337
175. Volpert, V.; Banerjee, M.; Sharma, S. Epidemic progression and vaccination in a heterogeneous population. application to the COVID-19 epidemic. *Ecological Complexity* **2021**, *47*, 100940. 1338–1339
176. Griffith, G.J.; Smith, G.D.; Manley, D.; Howe, L.D.; Owen, G. Interrogating structural inequalities in COVID-19 mortality in England and Wales. *J Epidemiol Community Health* **2021**, *75*, 1165–1171. 1340–1342
177. Melo, A.M.; Santos, M.C. Final size and partial distance estimate for a two-group SEIRD model. *Journal of Mathematical Biology* **2023**, *86*, 56. 1343–1344

178. Reingruber, J.; Papale, A.; Ruckly, S.; Timsit, J.F.; Holcman, D. Data-driven multiscale dynamical framework to control a pandemic evolution with non-pharmaceutical interventions. *PLoS One* **2023**, *18*, e0278882. 1345-1347
179. Olumoyin, K.; Khaliq, A.; Furati, K. Data-driven deep-learning algorithm for asymptomatic COVID-19 model with varying mitigation measures and transmission rate. *Epidemiologia* **2021**, *2*, 471–489. 1348-1350
180. Zhang, P.; Feng, K.; Gong, Y.; Lee, J.; Lomonaco, S.; Zhao, L. Usage of Compartmental Models in Predicting COVID-19 Outbreaks. *The AAPS Journal* **2022**, *24*, 98. 1351-1352
181. Anggriani, N.; Ndi, M.Z.; Amelia, R.; Suryaningrat, W.; Pratama, M.A.A. A mathematical COVID-19 model considering asymptomatic and symptomatic classes with waning immunity. *Alexandria Engineering Journal* **2022**, *61*, 113–124. 1353-1355
182. Anguelov, R.; Banasiak, J.; Bright, C.; Lubuma, J.; Ouifki, R. The big unknown: The asymptomatic spread of COVID-19. *Biomath* **2020**, *9*, ID–2005103. 1356-1357
183. Batistela, C.M.; Correa, D.P.; Bueno, Á.M.; Piqueira, J.R.C. SIRSi compartmental model for COVID-19 pandemic with immunity loss. *Chaos, Solitons & Fractals* **2021**, *142*, 110388. 1358-1359
184. Chen, X.; Huang, Z.; Wang, J.; Zhao, S.; Wong, M.C.S.; Chong, K.C.; He, D.; Li, J. Ratio of asymptomatic COVID-19 cases among ascertained SARS-CoV-2 infections in different regions and population groups in 2020: a systematic review and meta-analysis including 130 123 infections from 241 studies. *BMJ open* **2021**, *11*, e049752. 1360-1363
185. Aguiar, M.; Van-Dierdonck, J.B.; Mar, J.; Stollenwerk, N. The role of mild and asymptomatic infections on COVID-19 vaccines performance: a modeling study. *Journal of Advanced Research* **2022**, *39*, 157–166. 1364-1366
186. Postnikov, E.B. Estimation of COVID-19 dynamics “on a back-of-envelope”: Does the simplest SIR model provide quantitative parameters and predictions? *Chaos, Solitons & Fractals* **2020**, *135*, 109841. 1367-1369
187. Biswas, K.; Khaleque, A.; Sen, P. COVID-19 spread: Reproduction of data and prediction using a SIR model on Euclidean network. *arXiv preprint arXiv:2003.07063* **2020**. 1370-1371
188. Mehmood, K.; Bao, Y.; Petropoulos, G.P.; Abbas, R.; Abrar, M.M.; Mustafa, A.; Soban, A.; Saud, S.; Ahmad, M.; Hussain, I.; et al. Investigating connections between COVID-19 pandemic, air pollution and community interventions for Pakistan employing geoinformation technologies. *Chemosphere* **2021**, *272*, 129809. 1372-1375
189. Smith, A.P.; Williams, E.P.; Plunkett, T.R.; Selvaraj, M.; Lane, L.C.; Zaldondo, L.; Xue, Y.; Vogel, P.; Channappanavar, R.; Jonsson, C.B.; et al. Time-dependent increase in susceptibility and severity of secondary bacterial infections during SARS-CoV-2. *Frontiers in Immunology* **2022**, *13*, 894534. 1376-1379
190. Jenner, A.L.; Aogo, R.A.; Alfonso, S.; Crowe, V.; Smith, A.P.; Morel, P.A.; Davis, C.L.; Smith, A.M.; Craig, M. COVID-19 virtual patient cohort reveals immune mechanisms driving disease outcomes. *bioRxiv* **2021**. 1380-1382
191. Nordström, P.; Ballin, M.; Nordström, A. Risk of SARS-CoV-2 reinfection and COVID-19 hospitalisation in individuals with natural and hybrid immunity: a retrospective, total population cohort study in Sweden. *The Lancet Infectious Diseases* **2022**, *22*, 781–790. 1383-1385
192. Huang, L.; Lai, F.T.T.; Yan, V.K.C.; Cheng, F.W.T.; Cheung, C.L.; Chui, C.S.L.; Li, X.; Wan, E.Y.F.; Wong, C.K.H.; Hung, I.F.N.; et al. Comparing hybrid and regular COVID-19 vaccine-induced immunity against the Omicron epidemic. *npj Vaccines* **2022**, *7*, 162. 1386-1388
193. Pilz, S.; Theiler-Schwetz, V.; Trummer, C.; Krause, R.; Ioannidis, J.P. SARS-CoV-2 reinfections: Overview of efficacy and duration of natural and hybrid immunity. *Environmental research* **2022**, *209*, 112911. 1389-1391
194. Stein, C.; Nassereldine, H.; Sorensen, R.J.; Amlag, J.O.; Bisignano, C.; Byrne, S.; Castro, E.; Coberly, K.; Collins, J.K.; Dalos, J.; et al. Past SARS-CoV-2 infection protection against re-infection: a systematic review and meta-analysis. *The Lancet* **2023**, *401*, 833–842. 1392-1394
195. Ruan, S. Likelihood of survival of coronavirus disease 2019. *The Lancet Infectious Diseases* **2020**, *20*, 630–631. 1395-1396
196. Soubeyrand, S.; Ribaud, M.; Baudrot, V.; Allard, D.; Pommeret, D.; Roques, L. COVID-19 mortality dynamics: The future modelled as a (mixture of) past (s). *Plos one* **2020**, *15*, e0238410. 1397-1399
197. Kobayashi, T.; Jung, S.m.; Linton, N.M.; Kinoshita, R.; Hayashi, K.; Miyama, T.; Anzai, A.; Yang, Y.; Yuan, B.; Akhmetzhanov, A.R.; et al. Communicating the risk of death from novel coronavirus disease COVID-19, 2020. 1400-1401-1402

198. Jung, S.m.; Akhmetzhanov, A.R.; Hayashi, K.; Linton, N.M.; Yang, Y.; Yuan, B.; Kobayashi, T.; Kinoshita, R.; Nishiura, H. Real-time estimation of the risk of death from novel coronavirus (COVID-19) infection: inference using exported cases. *Journal of clinical medicine* **2020**, *9*, 523. 1403
1404
1405
1406
199. Ioannidis, J.P. Global perspective of COVID-19 epidemiology for a full-cycle pandemic. *European journal of clinical investigation* **2020**, *50*, e13423. 1407
1408
200. Ioannidis, J.P. Infection fatality rate of COVID-19 inferred from seroprevalence data. *Bulletin of the world health organization* **2021**, *99*, 19. 1409
1410
201. Ioannidis, J.P. Reconciling estimates of global spread and infection fatality rates of COVID-19: an overview of systematic evaluations. *European journal of clinical investigation* **2021**, *51*, e13554. 1411
1412
1413
202. Ioannidis, J.P.; Zonta, F.; Levitt, M. What Really Happened During the Massive SARS-CoV-2 Omicron Wave in China? *JAMA Internal Medicine* **2023**. 1414
1415
203. Mehraeen, E.; Karimi, A.; Barzegary, A.; Vahedi, F.; Afsahi, A.M.; Dadras, O.; Moradmand-Badie, B.; Alinaghi, S.A.S.; Jahanfar, S. Predictors of mortality in patients with COVID-19—a systematic review. *European journal of integrative medicine* **2020**, *40*, 101226. 1416
1417
1418
204. Demongeot, J.; Griette, Q.; Magal, P.; Webb, G. Modeling vaccine efficacy for COVID-19 outbreak in New York city. *Biology* **2022**, *11*, 345. 1419
1420
205. Jarumaneeroj, P.; Dusadeerungsikul, P.O.; Chotivanich, T.; Nopsopon, T.; Pongpirul, K. An epidemiology-based model for the operational allocation of COVID-19 vaccines: A case study of Thailand. *Computers & industrial engineering* **2022**, *167*, 108031. 1421
1422
1423
206. Marinov, T.T.; Marinova, R.S. Adaptive SIR model with vaccination: Simultaneous identification of rates and functions illustrated with COVID-19. *Scientific Reports* **2022**, *12*, 15688. 1424
1425
207. Ioannidis, J.P. COVID-19 vaccination in children and university students. *European journal of clinical investigation* **2021**, *51*, e13678. 1426
1427
208. Ioannidis, J.P. Estimating conditional vaccine effectiveness. *European Journal of Epidemiology* **2022**, *37*, 885–890. 1428
1429
209. He, D.; Ali, S.T.; Fan, G.; Gao, D.; Song, H.; Lou, Y.; Zhao, S.; Cowling, B.J.; Stone, L. Evaluation of effectiveness of global COVID-19 vaccination campaign. *Emerging Infectious Diseases* **2022**, *28*, 1873. 1430
1431
1432
210. Hale, T.; Angrist, N.; Hale, A.J.; Kira, B.; Majumdar, S.; Petherick, A.; Phillips, T.; Sridhar, D.; Thompson, R.N.; Webster, S.; et al. Government responses and COVID-19 deaths: Global evidence across multiple pandemic waves. *PLoS One* **2021**, *16*, e0253116. 1433
1434
1435
211. Acuña-Zegarra, M.A.; Santana-Cibrian, M.; Velasco-Hernandez, J.X. Modeling behavioral change and COVID-19 containment in Mexico: A trade-off between lockdown and compliance. *Mathematical biosciences* **2020**, *325*, 108370. 1436
1437
1438
212. Wu, J.; Tang, B.; Bragazzi, N.L.; Nah, K.; McCarthy, Z. Quantifying the role of social distancing, personal protection and case detection in mitigating COVID-19 outbreak in Ontario, Canada. *Journal of mathematics in industry* **2020**, *10*, 1–12. 1439
1440
1441
213. Rozhnova, G.; van Dorp, C.H.; Bruijning-Verhagen, P.; Bootsma, M.C.; van de Wijert, J.H.; Bonten, M.J.; Kretzschmar, M.E. Model-based evaluation of school-and non-school-related measures to control the COVID-19 pandemic. *Nature communications* **2021**, *12*, 1614. 1442
1443
1444
214. Teslya, A.; Pham, T.M.; Godijk, N.G.; Kretzschmar, M.E.; Bootsma, M.C.; Rozhnova, G. Impact of self-imposed prevention measures and short-term government-imposed social distancing on mitigating and delaying a COVID-19 epidemic: A modelling study. *PLoS medicine* **2020**, *17*, e1003166. 1445
1446
1447
1448
215. Liu, K.; Lou, Y. Optimizing COVID-19 vaccination programs during vaccine shortages. *Infectious Disease Modelling* **2022**, *7*, 286–298. 1449
1450
216. Coccia, M. Optimal levels of vaccination to reduce COVID-19 infected individuals and deaths: A global analysis. *Environmental research* **2022**, *204*, 112314. 1451
1452
217. Halim, M.; Halim, A.; Tjhin, Y. COVID-19 vaccination efficacy and safety literature review. *J Clin Med Res* **2021**, *3*, 1–10. 1453
1454
218. Zhou, W.; Wang, A.; Xia, F.; Xiao, Y.; Tang, S. Effects of media reporting on mitigating spread of COVID-19 in the early phase of the outbreak. *Mathematical Biosciences and Engineering* **2020**, *17*, 2693–2707. 1455
1456
1457
219. Monod, M.; Blenkinsop, A.; Xi, X.; Hebert, D.; Bershan, S.; Tietze, S.; Baguelin, M.; Bradley, V.C.; Chen, Y.; Coupland, H.; et al. Age groups that sustain resurging COVID-19 epidemics in the United States. *Science* **2021**, *371*, eabe8372. 1458
1459
1460

220. Tran Kiem, C.; Bosetti, P.; Paireau, J.; Crepey, P.; Salje, H.; Lefrancq, N.; Fontanet, A.; Benamouzig, D.; Boëlle, P.Y.; Desenclos, J.C.; et al. SARS-CoV-2 transmission across age groups in France and implications for control. *Nature communications* **2021**, *12*, 6895. 1461-1463
221. Van Zandvoort, K.; Jarvis, C.I.; Pearson, C.A.; Davies, N.G.; Ratnayake, R.; Russell, T.W.; Kucharski, A.J.; Jit, M.; Flasche, S.; Eggo, R.M.; et al. Response strategies for COVID-19 epidemics in African settings: a mathematical modelling study. *BMC medicine* **2020**, *18*, 1–19. 1464-1466
222. Ghafari, M.; Hejazi, B.; Karshenas, A.; Dascalu, S.; Kadvidar, A.; Khosravi, M.A.; Abbasalipour, M.; Heydari, M.; Zeinali, S.; Ferretti, L.; et al. Lessons for preparedness and reasons for concern from the early COVID-19 epidemic in Iran. *Epidemics* **2021**, *36*, 100472. 1467-1469
223. Anderson, S.J.; Garnett, G.P.; Enstone, J.; Hallett, T.B. The importance of local epidemic conditions in monitoring progress towards HIV epidemic control in Kenya: a modelling study. *Journal of the International AIDS Society* **2018**, *21*, e25203. 1470-1472
224. Kombe, I.K.; Munywoki, P.K.; Baguelin, M.; Nokes, D.J.; Medley, G.F. Model-based estimates of transmission of respiratory syncytial virus within households. *Epidemics* **2019**, *27*, 1–11. 1473-1474
225. Prem, K.; Liu, Y.; Russell, T.W.; Kucharski, A.J.; Eggo, R.M.; Davies, N. The effect of control strategies to reduce social mixing on outcomes of the COVID-19 epidemic in Wuhan, China: a modelling study. *The Lancet Public Health* **2020**, *5*, e261–e270. 1475-1477
226. Kuo, C.L.; Pilling, L.C.; Atkins, J.L.; Masoli, J.A.; Delgado, J.; Tignanelli, C.; Kuchel, G.A.; Melzer, D.; Beckman, K.B.; Levine, M.E. COVID-19 severity is predicted by earlier evidence of accelerated aging. *Medrxiv* **2020**. 1478-1480
227. Polidori, M.C.; Sies, H.; Ferrucci, L.; Benzing, T. COVID-19 mortality as a fingerprint of biological age. *Ageing research reviews* **2021**, *67*, 101308. 1481-1482
228. Cao, X.; Li, W.; Wang, T.; Ran, D.; Davalos, V.; Planas-Serra, L.; Pujol, A.; Esteller, M.; Wang, X.; Yu, H. Accelerated biological aging in COVID-19 patients. *Nature communications* **2022**, *13*, 2135. 1483-1485
229. Alimohamadi, Y.; Taghdir, M.; Sepandi, M. Estimate of the basic reproduction number for COVID-19: a systematic review and meta-analysis. *Journal of Preventive Medicine and Public Health* **2020**, *53*, 151. 1486-1488
230. He, W.; Yi, G.Y.; Zhu, Y. Estimation of the basic reproduction number, average incubation time, asymptomatic infection rate, and case fatality rate for COVID-19: Meta-analysis and sensitivity analysis. *Journal of medical virology* **2020**, *92*, 2543–2550. 1489-1491
231. Billah, M.A.; Miah, M.M.; Khan, M.N. Reproductive number of coronavirus: A systematic review and meta-analysis based on global level evidence. *PloS one* **2020**, *15*, e0242128. 1492-1493
232. Zhao, S.; Lin, Q.; Ran, J.; Musa, S.S.; Yang, G.; Wang, W.; Lou, Y.; Gao, D.; Yang, L.; He, D.; et al. Preliminary estimation of the basic reproduction number of novel coronavirus (2019-nCoV) in China, from 2019 to 2020: A data-driven analysis in the early phase of the outbreak. *International journal of infectious diseases* **2020**, *92*, 214–217. 1494-1496
233. White, L.F.; Moser, C.B.; Thompson, R.N.; Pagano, M. Statistical estimation of the reproductive number from case notification data. *American Journal of Epidemiology* **2021**, *190*, 611–620. 1497-1500
234. Demongeot, J.; Oshinubi, K.; Rachdi, M.; Seligmann, H.; Thuderoz, F.; Waku, J. Estimation of daily reproduction numbers during the COVID-19 outbreak. *Computation* **2021**, *9*, 109. 1501-1502
235. Otto, S.P.; Day, T.; Arino, J.; Colijn, C.; Dushoff, J.; Li, M.; Mechai, S.; Van Domselaar, G.; Wu, J.; Earn, D.J.; et al. The origins and potential future of SARS-CoV-2 variants of concern in the evolving COVID-19 pandemic. *Current Biology* **2021**, *31*, R918–R929. 1503-1505
236. Yang, W.; Shaman, J.L. COVID-19 pandemic dynamics in South Africa and epidemiological characteristics of three variants of concern (Beta, Delta, and Omicron). *Elife* **2022**, *11*. 1506-1507
237. Miller, J.K.; Elenberg, K.; Dubrawski, A. Forecasting emergence of COVID-19 variants of concern. *PLoS One* **2022**, *17*, e0264198. 1508-1509
238. Hussein, T.; Hammad, M.H.; Surakhi, O.; AlKhanafseh, M.; Fung, P.L.; Zaidan, M.A.; Wraith, D.; Ershaidat, N. Short-Term and long-term COVID-19 pandemic forecasting revisited with the emergence ofOMICRON variant in Jordan. *Vaccines* **2022**, *10*, 569. 1510-1512
239. Hatami, F.; Chen, S.; Paul, R.; Thill, J.C. Simulating and forecasting the COVID-19 spread in a US Metropolitan region with a spatial SEIR model. *International Journal of Environmental Research and Public Health* **2022**, *19*, 15771. 1513-1515
240. Rashed, E.A.; Kodera, S.; Hirata, A. COVID-19 forecasting using new viral variants and vaccination effectiveness models. *Computers in Biology and Medicine* **2022**, *149*, 105986. 1516-1517

-
241. Du, H.; Dong, E.; Badr, H.S.; Petrone, M.E.; Grubaugh, N.D.; Gardner, L.M. Incorporating
variant frequencies data into short-term forecasting for COVID-19 cases and deaths in the
USA: a deep learning approach. *Ebiomedicine* **2023**, *89*, 104482. 1518
1519
1520
242. Ioannidis, J.P.; Cripps, S.; Tanner, M.A. Forecasting for COVID-19 has failed. *International
journal of forecasting* **2022**, *38*, 423–438. 1521
1522